




# The $R^2$ -Higgs inflation with two Higgs doublets

Sung Mook Lee<sup>1,a</sup>, Tanmoy Modak<sup>2,b</sup> , Kin-ya Oda<sup>3,c</sup>, Tomo Takahashi<sup>4,d</sup>

<sup>1</sup> Department of Physics and IPAP and Lab for Dark Universe, Yonsei University, Seoul 03722, Korea

<sup>2</sup> Institut für Theoretische Physik, Universität Heidelberg, 69120 Heidelberg, Germany

<sup>3</sup> Department of Mathematics, Tokyo Woman's Christian University, Tokyo 167-8585, Japan

<sup>4</sup> Department of Physics, Saga University, Saga 840-8502, Japan

Received: 4 November 2021 / Accepted: 28 December 2021 / Published online: 10 January 2022

© The Author(s) 2022

**Abstract** We study  $R^2$ -Higgs inflation in a model with two Higgs doublets in which the Higgs sector of the Standard Model is extended by an additional Higgs doublet, thereby four scalar fields are involved in the inflationary evolutions. We first derive the set of equations required to follow the inflationary dynamics in this two Higgs doublet model, allowing a nonminimal coupling between the Higgs-squared and the Ricci scalar  $R$ , as well as the  $R^2$  term in the covariant formalism. By numerically solving the system of equations, we find that, in parameter space where a successful  $R^2$ -Higgs inflation are realized and consistent with low energy constraints, the inflationary dynamics can be effectively described by a single slow-roll formalism even though four fields are involved in the model. We also argue that the parameter space favored by  $R^2$ -Higgs inflation requires nearly degenerate masses for  $m_H$ ,  $m_A$  and  $m_{H^\pm}$ , where H, A, and  $H^\pm$  are the extra CP even, CP odd, and charged Higgs bosons in the general two Higgs doublet model taking renormalization group evolutions of the parameters into account. Discovery of such heavy scalars at the Large Hadron Collider (LHC) are possible if they are in the sub-TeV mass range. Indirect evidences may also emerge at the LHCb and Belle-II experiments, however, to probe the quasi degenerate mass spectra one would likely require high luminosity LHC or future lepton colliders such as the International Linear Collider and the Future Circular Collider.

## 1 Introduction

The cosmic inflation [1–3] can successfully account for the observed flatness, horizon and the absence of the exotic-

relics and, can seed the condition required for the subsequent hot big bang via the reheating process. The primordial density perturbations generated during inflation [4–7] can subsequently develop into large scale structure of the Universe and the cosmic microwave background (CMB) anisotropies measured by experiments such as Planck [23]. While the cosmic inflation is indeed a well established paradigm for the very early epoch of the Universe, however, the mechanism behind it is still unknown.

The Higgs inflation [8–14] (for earlier works which employed essentially the same idea, see [15–22]) is one of the candidates that best fits the CMB data [23] and, draws significant attention due to its direct connection to the physics at the LHC. In the Standard Model (SM) Higgs inflation, the Higgs field  $\Phi$  couples to the Ricci scalar  $R$  via  $\xi \Phi^\dagger \Phi R$  term, where  $\xi$  is dimensionless nonminimal coupling, and can account for the amplitude of the primordial perturbation along with the spectral index and the tensor-to-scalar ratio within the experimentally measured values [23]. While the Higgs inflation can fit the CMB data without requiring any additional degrees of freedom between the electroweak and Planck scale, however, a unitarity violating scale emerges below the Planck scale [24–27]. Because the energy scale for inflation lies below such cut-off scale, it does not pose any problem for inflationary dynamics during the inflation [10]. However, during preheating stage i.e., when the inflaton field oscillates around the potential minima, longitudinal gauge bosons with momenta beyond the unitarity cut-off scale are produced violently [28–30]. The perturbative unitarity of the Higgs inflation can be restored up to the Planck scale by introducing additional scalars at the inflationary scale [31, 32] or, by scalaron degree of freedom due to the presence of  $R^2$  term ( $R^2$ -Higgs inflation) in the Jordan frame [33] (see also for e.g. [34–43]).

In this article we study the  $R^2$ -Higgs inflation in the general two Higgs doublet model (g2HDM) where the SM is

<sup>a</sup> e-mail: [sungmook.lee@yonsei.ac.kr](mailto:sungmook.lee@yonsei.ac.kr)

<sup>b</sup> e-mail: [tanmoyy@thphys.uni-heidelberg.de](mailto:tanmoyy@thphys.uni-heidelberg.de) (corresponding author)

<sup>c</sup> e-mail: [odakin@gmail.com](mailto:odakin@gmail.com)

<sup>d</sup> e-mail: [tomot@cc.saga-u.ac.jp](mailto:tomot@cc.saga-u.ac.jp)

extended by an additional scalar doublet  $\Phi'$ . After the discovery of 125 GeV Higgs boson  $h$  [44, 45] the existence of additional scalar doublet seems plausible as all known fermions appear in nature with more than one generation. In addition, it is known that the electroweak vacuum is metastable for the current central values of the SM parameters [46], especially for top quark mass, which also could pose a threat for the SM Higgs inflation.<sup>1</sup> If the scale of the instability is smaller than the required mass scale of the scalaron  $M \gtrsim 10^{-5} M_P$  ( $M_P \equiv 1/\sqrt{8\pi G} \simeq 2.4 \times 10^{18}$  GeV) to fit the Planck measurement of the scalar power spectrum amplitude, just adding  $R^2$  term may not be enough to solve the problem [33, 36, 49]. This partially motivates us to consider extension of the Higgs sector, in addition to the  $R^2$  term of the SM Higgs inflation.

In this paper we study the inflationary dynamics and primordial fluctuations in the  $R^2$ -Higgs inflation in the framework of the g2HDM based on the covariant formalism. The work here also remedies the shortcomings of Ref. [50] where inflationary dynamics was also under scrutiny due to the unitarity violation by the required large nonminimal couplings  $\mathcal{O}(10^4 - 6 \times 10^4)$  as in the SM.<sup>2</sup> As we will argue, the parameter sets consistent with current observations of Planck and low energy constraints give almost the same predictions for primordial power spectrum, we take four benchmark points as representative ones to show the inflationary dynamics and the evolutions of perturbations. For two benchmark points (PBs), we take the nonminimal coupling of the scalaron degree of freedom to be much larger than Higgs nonminimal coupling ( $R^2$ -like scenario) i.e., akin to the original Starobinsky model [55], whereas for the other BPs, we take both the Higgs and scalaron nonminimal couplings relatively large (denoted as mixed  $R^2$ -Higgs scenario). We further provide sub-TeV parameter space for  $R^2$ -Higgs inflation in the g2HDM that can satisfy all observational constraints from Planck 2018 [23] and discuss the possibility of probing such parameter space at the current experiment such as the LHC and future lepton colliders such as the International Linear Collider (ILC) and the Future Circular Collider (FCC-ee). Moreover, indirect evidences of such additional Higgs bosons may also emerge in the ongoing flavor experiments such as LHCb and Belle-II.

The paper is organized as follows. In Sect. 2 we first discuss the model framework of the g2HDM. We outline the framework to follow the inflationary dynamics and perturbations based on the covariant formalism in Sect. 3 followed by numerical study in Sect. 4. We discuss possible discoveries and probes for the parameter space required for  $R^2$ -Higgs

inflation at the collider experiments in Sect. 5. We summarize our results with an outlook in Sect. 6.

## 2 Model framework

The most general  $CP$ -conserving two Higgs doublet model<sup>3</sup> potential can be given in the Higgs basis as [58, 59]

$$V(\Phi, \Phi') = \mu_{11}^2 |\Phi|^2 + \mu_{22}^2 |\Phi'|^2 - (\mu_{12}^2 \Phi^\dagger \Phi' + h.c.) + \frac{\eta_1}{2} |\Phi|^4 + \frac{\eta_2}{2} |\Phi'|^4 + \eta_3 |\Phi|^2 |\Phi'|^2 + \eta_4 |\Phi^\dagger \Phi'|^2 + \left[ \frac{\eta_5}{2} (\Phi^\dagger \Phi')^2 + (\eta_6 |\Phi|^2 + \eta_7 |\Phi'|^2) \Phi^\dagger \Phi' + h.c. \right], \tag{1}$$

where the vacuum expectation value  $v$  arises from the doublet  $\Phi$  via the minimization condition  $\mu_{11}^2 = -\frac{1}{2}\eta_1 v^2$ , while we take  $\langle \Phi \rangle = (0, v/\sqrt{2})^T, \langle \Phi' \rangle = 0$  (hence  $\mu_{22}^2 > 0$ ), and  $\eta_i$ s are quartic couplings. A second minimization condition,  $\mu_{12}^2 = \frac{1}{2}\eta_6 v^2$ , removes  $\mu_{12}^2$ , and the total number of parameters are reduced to nine. The mixing angle  $\gamma$  is given by, when diagonalizing the mass-squared matrix for  $h, H$ ,

$$c_\gamma^2 = \frac{\eta_1 v^2 - m_h^2}{m_H^2 - m_h^2}, \quad \sin 2\gamma = \frac{2\eta_6 v^2}{m_H^2 - m_h^2}, \tag{2}$$

with shorthand notation  $c_\gamma = \cos \gamma$ . The physical scalar masses can be expressed in terms of the parameters in Eq. (13),

$$m_{h,H}^2 = \frac{1}{2} \left[ m_A^2 + (\eta_1 + \eta_5)v^2 \mp \sqrt{(m_A^2 + (\eta_5 - \eta_1)v^2)^2 + 4\eta_6^2 v^4} \right], \tag{3}$$

$$m_A^2 = \frac{1}{2}(\eta_3 + \eta_4 - \eta_5)v^2 + \mu_{22}^2, \tag{4}$$

$$m_{H^\pm}^2 = \frac{1}{2}\eta_3 v^2 + \mu_{22}^2. \tag{5}$$

The scalars  $h, H, A$  and  $H^\pm$  couple to fermions by [58]

$$\mathcal{L} = -\frac{1}{\sqrt{2}} \sum_{F=U,D,L} \bar{F}_i \left[ (-\lambda_{ij}^F s_\gamma + \rho_{ij}^F c_\gamma) h + (\lambda_{ij}^F c_\gamma + \rho_{ij}^F s_\gamma) H - i \operatorname{sgn}(Q_F) \rho_{ij}^F A \right] P_R F_j - \bar{U}_i \left[ (V\rho^D)_{ij} P_R - (\rho^{U^\dagger} V)_{ij} P_L \right] D_j H^+ - \bar{\nu}_i \rho_{ij}^L P_R L_j H^+ + h.c., \tag{6}$$

<sup>1</sup> If one demands the stability up to Planck scale, the required upper limit on the top quark pole mass is  $m_t^{\text{pole}} \lesssim 171.4$  GeV [47], which is consistent at  $1.6\sigma$  with the current combined result  $172.5 \pm 0.7$  GeV [48].

<sup>2</sup> See also Refs. [51–54] for discussions on inflation in the 2HDM.

<sup>3</sup> See Refs. [56, 57] for pedagogical reviews on the two Higgs doublet model.

where  $P_{L,R} \equiv (1 \mp \gamma_5)/2$ ,  $i, j = 1, 2, 3$  are generation indices,  $V$  is Cabibbo–Kobayashi–Maskawa matrix,  $s_\gamma = \sin \gamma$  and  $U = (u, c, t)$ ,  $D = (d, s, b)$ ,  $L = (e, \mu, \tau)$  and  $\nu = (\nu_e, \nu_\mu, \nu_\tau)$  are vectors in flavor space. The matrices  $\lambda_{ij}^F (= \sqrt{2}m_i^F/\nu)$  are real and diagonal, whereas  $\rho_{ij}^F$  are in general complex and non-diagonal.

In general, one may allow data to constrain different elements of  $\rho_{ij}^F$  matrices. However, it is likely that  $\rho_{ij}^F$  matrices follow the same flavor organization principle as in SM. This means  $\rho_{ij}^F \sim \lambda_{ii}^F$  i.e.,  $\rho_{it}^U \sim \lambda_t^U$ ,  $\rho_{bb}^D \sim \lambda_b^D$ ,  $\rho_{\tau\tau}^L \sim \lambda_\tau^L$  etc. with suppressed off diagonal elements. While apart from getting involved in the RGE, the additional Yukawa couplings  $\rho_{ij}^F$  do not play any major role in the inflationary dynamics, they are essential for possible discovery of the heavy Higgs bosons  $H, A$  and  $H^\pm$ . For all practical purposes we shall set all  $\rho_{ij}^F$  couplings to zero except for  $\rho_{it}^U$  and  $\rho_{tc}^U$  throughout this paper, however, the impact of turning on different  $\rho_{ij}^F$  couplings and their constraints will be discussed in Sect. 5 of this paper. In this work, we primarily focus on the sub-TeV mass range i.e.  $m_A, m_H, m_{H^\pm}$  in the range of 200–800 GeV in the urge of finding complementarity between  $R^2$ -Higgs inflation and the ongoing collider experiments such as the LHC, although heavier Higgs bosons are also possible in principle.

### 3 Inflationary dynamics of $R^2$ -Higgs inflation

In this section, we outline the required formalism for  $R^2$ -Higgs inflation in the g2HDM and analyze perturbation theory using the covariant formalism [60–67].

#### 3.1 The action in $R^2$ -Higgs inflation

The model can be understood as a particle-physics motivated generalization of  $R^2$ -Higgs inflation model. In the Jordan frame, the action is given by

$$S = \int d^4x \sqrt{-g_J} \left[ -g_J^{\mu\nu} \left( \partial_\mu \Phi^\dagger \partial_\nu \Phi + \partial_\mu \Phi'^\dagger \partial_\nu \Phi' \right) + \left( \frac{M_P^2}{2} + \xi_{11} |\Phi|^2 + \xi_{22} |\Phi'|^2 + (\xi_{12} \Phi^\dagger \Phi' + h.c.) \right) R_J + \frac{\xi_R}{4} R_J^2 - V(\Phi, \Phi') \right], \tag{7}$$

with  $g_J = \det g_{J\mu\nu}$ , Ricci scalar  $R_J$  and  $(-1, +1, +1, +1)$  metric convention and we adopt the natural unit  $\hbar = c = 1$ . The  $\xi_{ij}$ s are nonminimal couplings between Higgs' and Ricci Scalar and  $\xi_R$  is the self coupling of Ricci scalar. In the following we would turn off the nonminimal coupling  $\xi_{12} = \xi_{22} = 0$  for simplicity however we shall return to their impacts in the latter half of the paper.

We introduce an auxiliary field  $s$  for which the action in Eq. (7) can be rewritten as

$$S = \int d^4x \sqrt{-g_J} \left[ \left( \frac{M_P^2}{2} + \xi_{11} |\Phi|^2 + \frac{1}{2} \xi_{R s} \right) R_J - \frac{\xi_R}{4} s^2 - g_J^{\mu\nu} \left( \partial_\mu \Phi^\dagger \partial_\nu \Phi + \partial_\mu \Phi'^\dagger \partial_\nu \Phi' \right) - V(\Phi, \Phi') \right], \tag{8}$$

such that the variation of the action with respect to  $s$  gives  $s = R_J$ . For inflationary dynamics we choose the Higgs fields in the electromagnetic preserving direction:

$$\Phi = \frac{1}{\sqrt{2}} \begin{pmatrix} 0 \\ \rho_1 \end{pmatrix} \quad \text{and} \quad \Phi' = \frac{1}{\sqrt{2}} \begin{pmatrix} 0 \\ \rho_2 + i\rho_3 \end{pmatrix}. \tag{9}$$

We now perform the Weyl transformation to find the action in Einstein frame via

$$g_{\mu\nu} = F^2 g_{J\mu\nu}, \tag{10}$$

where the conformal factor  $F^2$  reads as

$$F^2 = 1 + \frac{\xi_{11} \rho_1^2 + \xi_{R s}}{M_P^2}. \tag{11}$$

The action of Eq. (8) can be written in the Einstein frame as

$$S_E = \int d^4x \sqrt{-g} \left[ \frac{M_P^2}{2} R - \frac{3M_P^2}{4} (\partial_\mu \log(F^2))^2 - \frac{1}{2} \frac{(\partial_\mu \rho_1)^2 + (\partial_\mu \rho_2)^2 + (\partial_\mu \rho_3)^2}{F^2} - V_E \right], \tag{12}$$

where

$$V_E = \frac{V(\rho_1, \rho_2, \rho_3) + 2\xi_{R s} s^2}{8F^4}, \tag{13}$$

with

$$V(\rho_1, \rho_2, \rho_3) = \left[ \tilde{\eta}_1 \rho_1^4 + \tilde{\eta}_2 (\rho_2^2 + \rho_3^2)^2 + 2\tilde{\eta}_5 (\rho_2^2 - \rho_3^2) \rho_1^2 + 2(\tilde{\eta}_3 + \tilde{\eta}_4) (\rho_2^2 + \rho_3^2) \rho_1^2 + 4\rho_2 \rho_1 \left\{ \tilde{\eta}_6 \rho_1^2 + \tilde{\eta}_7 (\rho_2^2 + \rho_3^2) \right\} \right]. \tag{14}$$

Here,  $\tilde{\eta}_i$ s correspond to the renormalization group evolution (RGE) of the parameters  $\eta_i$  at the inflationary scale  $\sim O(H)$ . Details of the running of the parameters are discussed in Sect. 4.

Let us perform following field redefinition [51]:

$$\varphi = \sqrt{\frac{3}{2}} M_P \ln(F^2), \tag{15}$$

resulting in a simple form of the action

$$S_E = \int d^4x \sqrt{-g} \left[ \frac{R}{2} - \frac{1}{2} G_{IJ} g^{\mu\nu} \partial_\mu \phi_I \partial_\nu \phi_J - V_E(\phi^I) \right], \tag{16}$$

where  $\phi^I = \{\varphi, \rho_1, \rho_2, \rho_3\}$  and  $G_{IJ}$  is field space metric, with only non-vanishing components are diagonal:

$$G_{\phi_1\phi_1} = 1, \quad G_{\phi_2\phi_2} = G_{\phi_3\phi_3} = G_{\phi_4\phi_4} = e^{-\sqrt{\frac{2}{3}} \frac{\varphi}{M_P}}. \tag{17}$$

Finally, we have the following action in the Einstein frame as

$$S_E = \int d^4x \sqrt{-g} \left[ \frac{M_P^2}{2} R - \frac{1}{2} (\partial_\mu \varphi)^2 - \frac{1}{2} e^{-\sqrt{\frac{2}{3}} \frac{\varphi}{M_P}} \times ((\partial_\mu \rho_1)^2 + (\partial_\mu \rho_2)^2 + (\partial_\mu \rho_3)^2) - V_E \right], \tag{18}$$

with

$$V_E(\varphi, \rho_1, \rho_2, \rho_3) = \frac{1}{8} e^{-2\sqrt{\frac{2}{3}} \frac{\varphi}{M_P}} \left[ V(\rho_1, \rho_2, \rho_3) + 2 \frac{M_P^4}{\xi_R} \times \left( e^{\sqrt{\frac{2}{3}} \frac{\varphi}{M_P}} - 1 - \frac{\xi_{11}}{M_P^2} \rho_1^2 \right)^2 \right]. \tag{19}$$

During numerical analysis, to remain in the perturbative regime, we also demand the upper bound on the scalaron mass as discussed in Refs. [33,36,49].

The equation of motions for the fields  $\phi^I$  can also be found by varying the action in Eq. (16) with respect to  $\phi^I$  as

$$g^{\mu\nu} \partial_\nu \partial_\mu \phi^I + g^{\mu\nu} \Gamma_{JK}^I \partial_\mu \phi^J \partial_\nu \phi^K - G^{IK} V_{E,K} = 0, \tag{20}$$

where  $\Gamma_{JK}^I(\phi^M)$  is the Christoffel symbol for the field space manifold  $G^{IK}$  and  $V_{E,K}$  denotes derivative of  $V_E$  with respect to field  $\phi^K$ . Explicit elements of  $\Gamma_{JK}^I$  in our model are given in the Appendix A. The background dynamics is governed by the Friedmann equations:

$$H^2 = \frac{1}{3M_P^2} \left( \frac{1}{2} G_{IJ} \dot{\phi}^I \dot{\phi}^J + V_E(\phi^I) \right), \tag{21}$$

$$\dot{H} = -\frac{1}{2M_P^2} G_{IJ} \dot{\phi}^I \dot{\phi}^J, \tag{22}$$

where an overdot represents the derivative with respect to time.

### 3.2 Background dynamics and the perturbation theory: covariant formalism

In this section we outline the covariant formalism [60–68] for our inflationary model, which includes four scalar fields

$\phi^I = \{\varphi, \rho_1, \rho_2, \rho_3\}$ . We closely follow the formalism for multi-field inflation as discussed in Ref. [68]. We divide the fields into classical background part ( $\bar{\varphi}^I$ ) and perturbation part ( $\delta\phi^I$ ) as

$$\phi^I(x^\mu) = \bar{\varphi}^I(t) + \delta\phi^I(x^\mu). \tag{23}$$

The perturbed spatially flat Friedmann-Robertson-Walker (FRW) metric can be expanded as [69–71]

$$ds^2 = -(1 + 2A)dt^2 + 2a(t)(\partial_i B)dx^i dt + a(t)^2 [(1 - 2\psi)\delta_{ij} + 2\partial_i \partial_j E] dx^i dx^j, \tag{24}$$

where  $a(t)$  is scale factor and  $t$  is the cosmic time.  $A, B, \psi$  and  $E$  characterize the scalar metric perturbations.

The  $\phi^I(x^\mu)$  field value in Eq. (23) depends on the background field value  $\bar{\varphi}^I(t)$  and, gauge dependent field fluctuation  $\delta\phi^I(x^\mu)$ . This motivates one to consider gauge independent Mukhanov–Sasaki variables for the field fluctuations expressed as [70,72,73]

$$Q^I = \mathcal{Q}^I + \frac{\dot{\phi}^I}{H} \psi, \tag{25}$$

with  $D_\kappa \phi^I|_{\kappa=0} = \frac{d\phi^I}{d\kappa}|_{\kappa=0} \equiv Q^I$  [62], where  $\kappa$  is the trajectory in the field space. The field fluctuations  $\delta\phi^I$  can be expressed in series of  $Q^I$  [62,74] as

$$\delta\phi^I = Q^I - \frac{1}{2} \Gamma_{JK}^I Q^J Q^K + \frac{1}{3!} (\Gamma_{MN}^I \Gamma_{JK}^N - \Gamma_{JK,M}^I) \times Q^J Q^K Q^M + \dots, \tag{26}$$

with Christoffel symbols  $\Gamma_{JK}^I$  evaluated with background field. We remark that, while  $\phi^I$  are not vectors in the field-space manifold,  $\mathcal{Q}^I, \dot{\phi}^I$  and  $Q^I$  all transform as vectors in the field-space manifold. At this point it is useful to define the covariant derivative of vectors  $S^I$  and  $S_I$  in the field-space as

$$\mathcal{D}_J S^I \equiv \partial_J S^I + \Gamma_{JK}^I S^K, \quad \mathcal{D}_J S_I \equiv \partial_J S_I - \Gamma_{IJ}^K S_K. \tag{27}$$

One can also define covariant derivative with respect to cosmic time  $t$  as [63,75–78]

$$\mathcal{D}_t S^I \equiv \dot{\phi}^J \mathcal{D}_J S^I = \dot{S}^I + \Gamma_{JK}^I S^J \dot{\phi}^K. \tag{28}$$

With these definitions, one can find that the background field equations can be written as

$$\mathcal{D}_t \dot{\phi}^I + 3H \dot{\phi}^I + G^{IK} V_{E,K} = 0. \tag{29}$$

Numerically we solve these set of background equations of motion for four fields  $\{\varphi, \rho_1, \rho_2, \rho_3\}$  along with Eq. (21).

While solving these equations we always check that the  $\dot{H}^2$  estimated from these solutions and, directly from the Eq. (22) are equal with high precision. Here, we remark that both in Eqs. (21) and (22), all field dependent quantities are evaluated with the background ones.

On the other hand, the equations for gauge invariant field fluctuations  $Q^I$  are given by

$$\mathcal{D}_t^2 Q^I + 3H\mathcal{D}_t Q^I + \left( \frac{k^2}{a^2} \delta_J^I + \mathcal{M}_J^I - \frac{1}{M_{\text{P}}^2 a^3} \times \mathcal{D}_t \left( \frac{a^3}{H} \dot{\phi}^I \dot{\phi}_J \right) \right) Q^J = 0, \tag{30}$$

where

$$\mathcal{M}_J^I = G^{IM} \mathcal{D}_J \mathcal{D}_M V_E - R_{MNI}^I \dot{\phi}^M \dot{\phi}^N \tag{31}$$

with  $R_{MNI}^I$  being field-space Riemann tensor, and we denote

$$\delta \mathcal{M}_J^I = -\frac{1}{M_{\text{P}}^2 a^3} \mathcal{D}_t \left( \frac{a^3}{H} \dot{\phi}^I \dot{\phi}_J \right) \tag{32}$$

for future use. Here in both Eqs. (29) and (30) quantities such as  $G^{IK}$ ,  $\Gamma_{JK}^I$ ,  $V_E$  etc. all are evaluated with the background quantities.

One can re-express Eqs. (21) and (22) as

$$H^2 = \frac{1}{3M_{\text{P}}^2} \left( \frac{1}{2} \dot{\sigma}^2 + V_E \right), \tag{33}$$

$$\dot{H} = -\frac{1}{2M_{\text{P}}^2} \dot{\sigma}^2, \tag{34}$$

where  $\dot{\sigma}$  is the length of the velocity vector  $\dot{\phi}^I$  in field-space defined as

$$\dot{\sigma} = \sqrt{G_{IJ} \dot{\phi}^I \dot{\phi}^J}. \tag{35}$$

We also introduce a unit vector  $\hat{\sigma}^I$  given as

$$\hat{\sigma}^I = \frac{\dot{\phi}^I}{\dot{\sigma}}. \tag{36}$$

The equation of motion reads as

$$\ddot{\sigma} + 3H\dot{\sigma} + V_{E,\sigma} = 0, \tag{37}$$

where  $V_{E,\sigma} \equiv \hat{\sigma}^I V_{E,I}$ . Together with Eqs. (33) and (34), Eq. (37) simply conforms of a single-field model with canonically normalized kinetic term. The slow-roll parameters  $\epsilon$  and  $\eta_{\sigma\sigma}$  can be defined as

$$\epsilon \equiv -\frac{\dot{H}}{H^2} = \frac{3\dot{\sigma}^2}{\dot{\sigma}^2 + 2V_E}, \tag{38}$$

$$\eta_{\sigma\sigma} \equiv M_{\text{P}}^2 \frac{\mathcal{M}_{\sigma\sigma}}{V_E}, \tag{39}$$

where  $\mathcal{M}_{\sigma\sigma} \equiv \hat{\sigma}_I \hat{\sigma}^J \mathcal{M}_J^I = \hat{\sigma}^I \hat{\sigma}^J (\mathcal{D}_I \mathcal{D}_J V_E)$ . The energy density  $\varrho(t)$  and pressure  $p(t)$  of the scalar field multiplets can be written as

$$\varrho = \frac{1}{2} \dot{\sigma}^2 + V_E, \tag{40}$$

$$p = \frac{1}{2} \dot{\sigma}^2 - V_E. \tag{41}$$

The field space directions orthogonal to  $\hat{\sigma}^I$  are expressed as

$$\hat{s}^{IJ} = G^{IJ} - \hat{\sigma}^I \hat{\sigma}^J. \tag{42}$$

The  $\hat{\sigma}^I$  and  $\hat{s}^{IJ}$  vectors are related by the relations

$$\begin{aligned} \hat{\sigma}^I \hat{\sigma}_I &= 1, \\ \hat{s}^{IJ} \hat{s}_{IJ} &= N - 1, \\ \hat{\sigma}_I \hat{s}^{IJ} &= 0 \text{ for each } J, \end{aligned} \tag{43}$$

where  $N$  is the number of scalar fields which is four in our case.

One can now decompose the perturbations in the directions of  $\hat{\sigma}^I$  and  $\hat{s}^{IJ}$  as

$$Q_\sigma = \hat{\sigma}_I Q^I, \tag{44}$$

$$\delta s^I = \hat{s}_J^I Q^J, \tag{45}$$

where  $Q_\sigma$  and  $\delta s^I$  are respectively called adiabatic and entropy perturbations.

In our four field case, there are three independent  $\delta s^I$ s. It is convenient to define three additional unit vectors by which one can identify these independent entropy directions. Here we follow the decomposition as discussed in Ref. [68] which essentially can reproduce the kinematical basis of Refs. [63, 77, 78]. In this regard, we first define turning vector  $\omega^I$  which can be defined as the covariant rate of change of  $\hat{\sigma}^I$  i.e.,

$$\omega^I = \mathcal{D}_t \hat{\sigma}^I. \tag{46}$$

It is also clear that with the definition above the turning vector is orthogonal to the  $\hat{\sigma}^I$  i.e.  $\omega_I \hat{\sigma}^I = 0$ . The unit turning vector is defined as

$$\hat{\omega}^I = \frac{\omega^I}{\omega}, \tag{47}$$

with  $\omega = |\omega^I| = \sqrt{G_{IJ} \omega^I \omega^J}$ . We now can construct a new projection operator  $\gamma^{IJ}$

$$\gamma^{IJ} = G^{IJ} - \hat{\sigma}^I \hat{\sigma}^J - \hat{\omega}^I \hat{\omega}^J. \tag{48}$$



Next vector is defined as

$$\Pi^I = \frac{1}{\omega} \mathcal{M}_{\sigma J} \gamma^{IJ}, \tag{49}$$

with  $\mathcal{M}_{\sigma J} = \hat{\sigma}_I \mathcal{M}_J^I$ .  $\Pi^I$  is orthogonal to both  $\hat{\sigma}_I$  and  $\hat{\omega}_I$ . The corresponding unit vector can be defined as  $\hat{\pi}^I = \Pi^I / |\Pi^I|$  with  $|\Pi^I| = |\Pi^I|$  and, a projection operator defined as  $q^{IJ} = \gamma^{IJ} - \hat{\pi}^I \hat{\pi}^J$ . The final vector for our four field scenario is  $\tau^I$  which is defined as

$$\tau^I = \frac{1}{\Pi} \left( \mathcal{M}_{sJ} + \frac{\dot{\sigma}}{\omega} \hat{\sigma}^K \hat{\sigma}_N (\mathcal{D}_K \mathcal{M}_J^N) \right) q^{IJ}, \tag{50}$$

and its corresponding unit vector is  $\hat{\tau}^I = \tau^I / |\tau^I|$ . With the unit vectors  $\hat{\omega}^I, \hat{\pi}^I$  and  $\hat{\tau}^I$ , we now are ready to define three independent components of entropy perturbations as

$$Q_s = \hat{\omega}_I Q^I, \tag{51}$$

$$Q_u = \hat{\pi}_I Q^I, \tag{52}$$

$$Q_v = \hat{\tau}_I Q^I. \tag{53}$$

The gauge-invariant curvature perturbation  $\mathcal{R}$  is defined as [70,71]

$$\mathcal{R} = \psi - \frac{H}{\varrho + p} \delta q, \tag{54}$$

where  $\varrho$  and  $p$  are defined in Eqs. (40) and (41) and,  $\delta q$  is the energy density flux defined by  $T_i^0 \equiv \partial_i \delta q$ . Utilizing

$$\delta q = -G_{IJ} \dot{\phi}^I \delta \phi^J = -\dot{\sigma} \hat{\sigma}_I \delta \sigma^I, \tag{55}$$

and, Eqs. (23) and (44) we find that  $\mathcal{R}$  can be given by

$$\mathcal{R} = \frac{H}{\dot{\sigma}} Q_\sigma. \tag{56}$$

The normalized entropy perturbations [68,79–81] can be derived as

$$\mathcal{S} = \frac{H}{\dot{\sigma}} Q_s, \tag{57}$$

$$\mathcal{U} = \frac{H}{\dot{\sigma}} Q_u, \tag{58}$$

$$\mathcal{V} = \frac{H}{\dot{\sigma}} Q_v. \tag{59}$$

At this point we remark that in our numerical analysis we always check that the orthogonality conditions of Eq. (43) and, as well as for the other unit vectors  $\hat{\omega}^I, \hat{\pi}^I$  and  $\hat{\tau}^I$  as given in Ref. [68] are satisfied.

Our focus of interest is the power spectrum of the gauge invariant curvature perturbation defined as [70,82]

$$\langle \mathcal{R}(\mathbf{k}_1) \mathcal{R}(\mathbf{k}_2) \rangle = (2\pi)^3 \delta^{(3)}(\mathbf{k}_1 + \mathbf{k}_2) P_{\mathcal{R}}(k_1) \tag{60}$$

and  $P_{\mathcal{R}}(k) = |\mathcal{R}|^2$ . The dimensionless power spectrum for the adiabatic perturbation is given by

$$\mathcal{P}_{\mathcal{R}}(t; k) = \frac{k^3}{2\pi^2} P_{\mathcal{R}}(k). \tag{61}$$

Similarly the power spectrum for the entropy perturbations are expressed as

$$\mathcal{P}_{\mathcal{S}}(t; k) = \frac{k^3}{2\pi^2} |\mathcal{S}|^2, \tag{62}$$

$$\mathcal{P}_{\mathcal{U}}(t; k) = \frac{k^3}{2\pi^2} |\mathcal{U}|^2, \tag{63}$$

$$\mathcal{P}_{\mathcal{V}}(t; k) = \frac{k^3}{2\pi^2} |\mathcal{V}|^2. \tag{64}$$

In order to find the power spectrum of the adiabatic and entropy perturbations given in Eqs. (61)–(64), we utilize the quantities  $H, \epsilon$  and unit vectors such as  $\hat{\sigma}^I, \hat{\omega}^I$  etc. from the solutions of the Eqs. (21) and (29) while  $Q_\sigma, Q_s, Q_u$  and  $Q_v$  are evaluated using the solutions of mode equations from Eq. (30). For a given Fourier mode  $k$ , we calculate the different power spectra at the  $t = t_{\text{end}}$  numerically as a function of  $k$  as

$$P_{\mathcal{R}}(k) = P_{\mathcal{R}}(t_{\text{end}}; k), \tag{65}$$

$$P_{\mathcal{S}}(k) = P_{\mathcal{S}}(t_{\text{end}}; k), \tag{66}$$

$$P_{\mathcal{U}}(k) = P_{\mathcal{U}}(t_{\text{end}}; k), \tag{67}$$

$$P_{\mathcal{V}}(k) = P_{\mathcal{V}}(t_{\text{end}}; k), \tag{68}$$

where  $t_{\text{end}}$  denotes the time when inflation ends i.e. when  $\epsilon = 1$ .

The spectral index  $n_s$  of the power spectrum of the adiabatic fluctuations is defined as

$$n_s = 1 + \frac{d \ln P_{\mathcal{R}}(k)}{d \ln k}. \tag{69}$$

As will be discussed in the next section, although four fields are involved during inflation in our model, we argue that in the parameter space where Planck and low energy constraints are satisfied, the power spectrum can effectively be described by the single field-like inflation. In such a case, the spectral index can be calculated as

$$n_s(t_*) \approx 1 - 6\epsilon(t_*) + 2\eta_{\sigma\sigma}(t_*), \tag{70}$$

where  $t_*$  denotes the time when the reference scale exited the horizon and the tensor-to-scalar ratio is given by  $r = 16\epsilon$ .

**Table 1** Benchmark points chosen for our analysis. See text for details

BPs	$\tilde{\eta}_1$	$\tilde{\eta}_2$	$\tilde{\eta}_3$	$\tilde{\eta}_4$	$\tilde{\eta}_5$	$\tilde{\eta}_6$	$\tilde{\eta}_7$	$\xi_{11}$	$\xi_R$
<i>a</i>	0.72459	0.834059	-0.287252	0.489654	-0.010900	-0.510739	0.333532	1	$2.4 \times 10^9$
<i>b</i>	0.845674	1.281688	0.017365	0.611085	-0.776203	-0.361704	0.050345	1800	$2.25 \times 10^9$
<i>c</i>	2.08746	1.11479	2.56305	-1.93179	-0.0412796	-0.521398	-0.0743505	$10^{-3}$	$2.42 \times 10^9$
<i>d</i>	0.634249	2.98825	0.083228	0.087188	0.152301	-0.494063	0.679174	200	$2.4 \times 10^9$

**Table 2** The low energy parameters for the BPs shown in Table 1 along with the masses of heavy Higgs bosons and mixing angle  $c_\gamma$  between the CP even Higgs *h* and *H*

BPs	$\eta_1$	$\eta_2$	$\eta_3$	$\eta_4$	$\eta_5$	$\eta_6$	$\eta_7$	$m_{H^+}$	$m_A$ (GeV)	$m_H$ (GeV)	$\frac{\mu_{23}^2}{v^2}$ (GeV)	$c_\gamma$
<i>a</i>	0.258353	0.214212	-0.104774	0.321234	-0.00339535	-0.0474321	0.132779	424	436	435	3.017	0.0165
<i>b</i>	0.257981	0.363637	-0.026754	0.194828	-0.225193	-0.0337426	0.0418302	429	443	428	3.043	0.0122
<i>c</i>	0.259349	0.245545	0.469357	-0.579992	-0.014849	-0.050576	0.061887	347	322	321	1.756	0.0352
<i>d</i>	0.258161	0.40482	0.134086	0.028604	0.059236	-0.066433	0.086559	681	681	683	7.581	0.0089

To solve field fluctuations given in Eq. (30) we utilize the Bunch–Davies vacuum

$$Q^I(k\tau_c \rightarrow -\infty) = \sqrt{\frac{1}{2k}} e^{-ik\tau_c}. \tag{71}$$

Here  $\tau_c$  is conformal time related to cosmological time *t* via  $dt = a d\tau_c$ . Such exact initial conditions need to be imposed in the infinite past which is numerically impractical. Here we utilize the approximate initialization of the field fluctuations and impose them in the sufficiently past such that the Hubble parameter at that time remains approximately constant. The conditions is [83]

$$Q^I(t_{in}) \simeq \frac{H}{\sqrt{2k^3}} \left( i + \frac{k}{aH} \right) e^{i\frac{k}{aH}}, \tag{72}$$

where *k* is the corresponding Fourier mode.<sup>4</sup> One can also use the approximate initial condition as in Ref. [84]

$$Q^I(t_{in}) \simeq \sqrt{\frac{1}{2k}} e^{-i\frac{k}{aH}\zeta}, \tag{73}$$

where  $\zeta$  is a numerical prefactor which we assumed to be 100 to ensure the field fluctuations are initialized sufficiently early times i.e. well within sub-horizon scale for each *k* mode. We have also checked numerically that both these initial conditions as in Eqs. (72) and (73) give the same power spectrum.

<sup>4</sup> For each mode, we initialize  $Q^I$  about 5 *e*-foldings before they exit horizon.

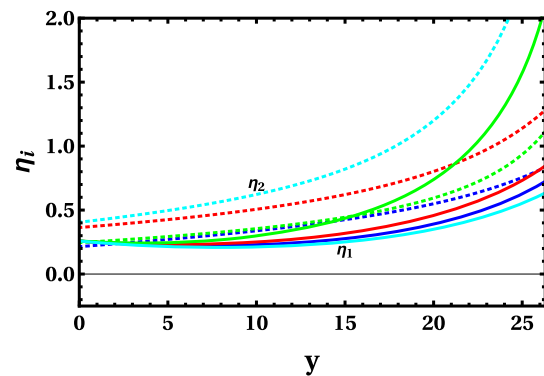


**Fig. 1** The running of  $\eta_1$  (solid) and  $\eta_2$  (dotted) for BPa, *b*, *c* and *d* are shown in blue, red, green and cyan lines respectively

## 4 Numerical results

### 4.1 Benchmark parameters and RG running

We consider four BPs for illustrative purpose which are shown in Table 1. The BPa and *c* correspond to scenarios where the Higgs nonminimal coupling  $\xi_{11}$  is small (denoted as  $R^2$ -like scenario). In BP*b* and BP*d* we consider parameter space where  $\xi_{11}$  is relatively large (denoted as mixed Higgs- $R^2$  like scenario). The low energy values for the corresponding parameters in Table 1 are presented at low scale ( $y = 0$ ) in Table 2.<sup>5</sup>

We require the dynamical parameters in Eq. (13) to satisfy the unitarity, perturbativity, and positivity constraints at the

<sup>5</sup> Here we provide the values of the quartic coupling  $\tilde{\eta}_i$  in Table 1 up to six decimal place. As one should expect, we remark that  $\tilde{\eta}_i$  values are highly sensitive to the corresponding low scale values of  $\eta_i$  as given in Table 2, for which we also consider six decimal place.

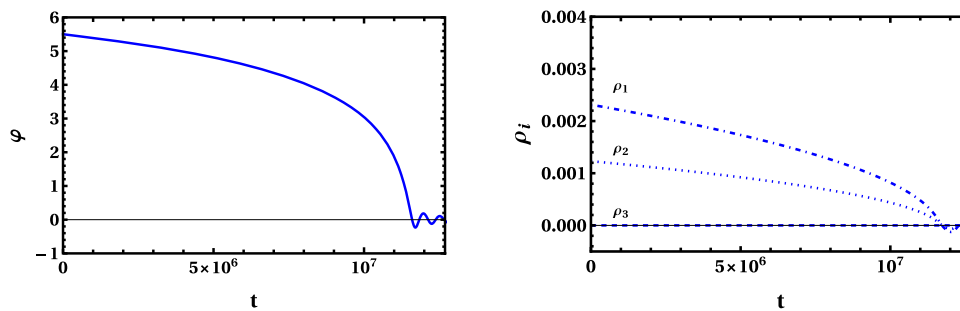


**Fig. 2** The time evolution of each background field  $\bar{\phi}^I$  in  $M_P$  units for the BP $a$ . The solid line in left panel correspond to the evolution of  $\varphi$  field while dot-dashed, dotted and dashed lines in right panels correspond to the evolution for  $\rho_1$ ,  $\rho_2$  and  $\rho_3$  fields respectively. To find the

background evolution we have used initial field values  $\varphi^1(t_{\text{in}}) = 5.5$ ,  $\varphi^2(t_{\text{in}}) = 0.002306$ ,  $\varphi^3(t_{\text{in}}) = 0.001227$  and  $\varphi^4(t_{\text{in}}) = 0$ . The prescription for finding the initial conditions are discussed in Appendix B and the analytic relations between  $\varphi$  and  $\rho_i$  are given in Appendix C

low scale ( $\mu = m_W$ ) for which we utilized 2HDMC [85]. To match the convention of 2HDMC, we take  $-\pi/2 \leq \gamma \leq \pi/2$ . For more details on the convention, parameter counting and low energy scanning we redirect readers to Refs. [86–89]. The low energy parameter sets for all BPs are further checked to satisfy the electroweak precision observables [90] within the  $2\sigma$  error [91]. While they do not directly play significant role in inflationary dynamics, we assumed  $\rho_{tt}^U = 0.5$ ,  $\rho_{tc}^U = 0.2$ ,  $\lambda_t^U = \sqrt{2} \frac{m_t}{v}$  at low scale and set all other Yukawa couplings to zero for simplicity for RG running.

It has been found that for parameter sets where  $|\eta_i| > 1$  at the low scale get generally excluded after imposing perturbativity criteria at the high scale [50]. Therefore, we simply adopt the strategy as in Ref. [50] and considered all benchmark points such that at low scale all  $|\eta_i|$ s are  $\leq 1$ .

For the RGE of the parameters in Eq. (13) as well as the Yukawa couplings  $\rho^F$  and  $\lambda^F$  in the Eq. (6) we utilized the  $\beta_x$  functions ( $\beta_x \equiv \partial x / \partial y$  with  $y \equiv \ln(\mu/m_W)$  where  $\mu$  is the renormalization scale) for g2HDM given in Ref. [92,93]. Here we take the low scale as  $y = 0$  and, take  $y \approx 26$  as inflationary scale or high scale.<sup>6</sup> After finding the parameters satisfying the constraints such as unitarity, perturbativity, stability and electroweak precision observables at the low (EW) scale, the same parameters are then evolved from low scale to high scale via the RG equations.

At the high scale, we also demand  $|\tilde{\eta}_i|$  and the Yukawa couplings to be within  $[-\pi, \pi]$ . To ensure the positivity of the potential in Eq. (14) the quartic couplings  $\tilde{\eta}_{1,2}$  are required to be positive, which is true for all four BPs as is evident from Fig. 1.

<sup>6</sup> To be precise in our numerical analysis we performed the RG evolution from  $y = 0$  to  $y = 26.3$ .

#### 4.2 Background dynamics and power spectrum

The background field evolutions are obtained by solving the Eqs. (20) and (21) with the initial field values at  $t = t_{\text{in}}$  providing  $e$ -folding number between CMB pivot scale and the time at the end of inflation  $\Delta \mathcal{N}_{\text{CMB}} \equiv \ln \frac{a(t_{\text{end}})}{a(t_{\text{CMB}})}$  larger than about 50-60. In what follows we set  $M_P = 1$ .

We show the time evolution of the background field  $\bar{\phi}^1 = \varphi$  for BP $a$  in the left panel of Fig. 2 in blue solid lines. In the right panel of Fig. 2 we plot the evolution of the background fields of  $\rho_1$ ,  $\rho_2$  and  $\rho_3$  by dot-dashed, dotted and dashed lines respectively. For the sake of illustration here we only provide figures for BP $a$  however we have checked other BPs also produce similar trajectories and inflationary dynamics. The evolutions of  $H$  (in  $M_P$  unit) and  $\epsilon$  are displayed in Fig. 3 in the left and right panels respectively. Inflation ends via breakdown of slow-roll condition i.e. when  $\epsilon(t_{\text{end}}) = 1$ .

Instead of  $t$ , we interchangeably use the number of  $e$ -foldings before the end of inflation

$$\mathcal{N} \equiv \ln \frac{a(t)}{a(t_{\text{end}})} \quad (74)$$

as a cosmological evolution variable to understand the inflationary dynamics. With this definition,  $t_{\text{end}}$  corresponds to zero  $e$ -foldings, whereas negative and positive  $\mathcal{N}$  denote the amount of  $e$ -foldings before and after the end of inflation respectively.

At the pivot scale  $k = k_*$ , the amplitude of  $\mathcal{P}_{\mathcal{R}}(k)$  should match the scalar amplitude measurement of Planck 2018  $A_s = (2.099 \pm 0.014) \times 10^{-9}$  at 68% CL [23]. We find that the pivot scale  $k_*$  exit horizon at around  $\mathcal{N} \sim -57$  for all BPs. However, it should be reminded that the relation between the number of  $e$ -foldings before the end of inflation and the pivot scale  $k_*$  depends on the thermal history after inflation.

In Fig. 4 we plot the power spectrum of the curvature perturbation  $\mathcal{P}_{\mathcal{R}}(k)$  vs  $\log_{10}(k/k_*)$  for BP $a$ , which shows



**Fig. 3** The evolution of  $H/M_P$  (left) and  $\epsilon$  (right) with respect to  $\mathcal{N}$  for BP $a$

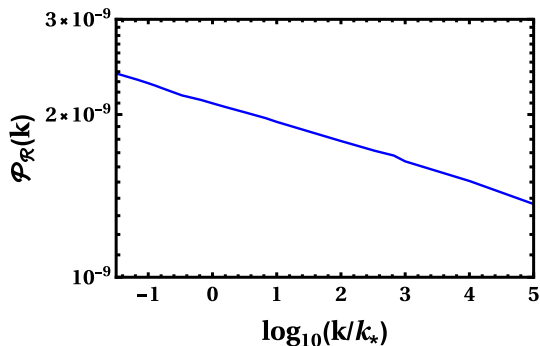
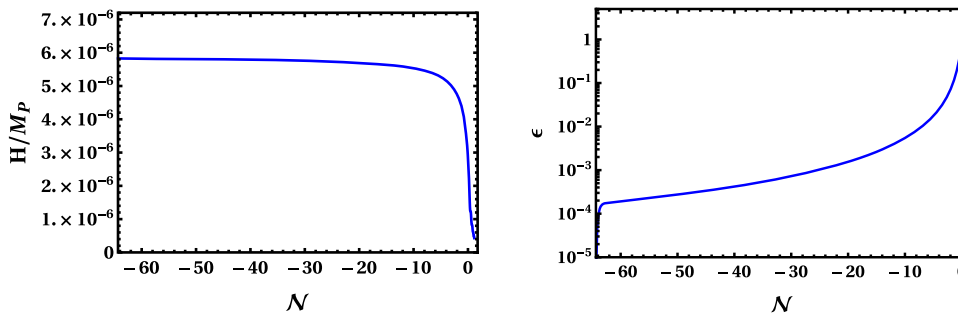


**Fig. 4** The power spectrum  $\mathcal{P}_{\mathcal{R}}(k)$  for the curvature perturbation as given in Eq. (65) for BP $a$  for illustration

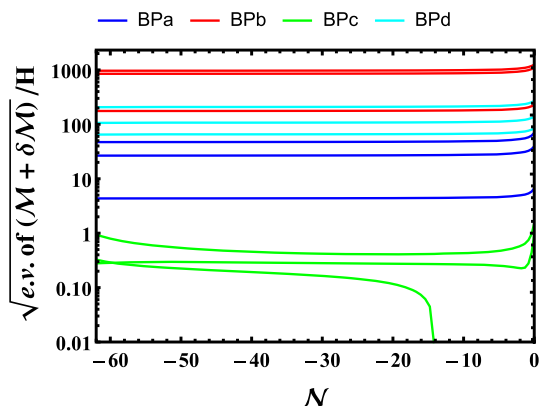


**Fig. 5** The square roots of the eigenvalues of  $\mathcal{M}_J^I + \delta\mathcal{M}_J^I$  in Eq. (30) for three heavy modes for four BPs during the inflation normalized by the Hubble parameter  $H$

nearly scale invariant but clearly red-tilted nature. We find that the entropy perturbations  $\mathcal{P}_{\mathcal{S}}(k)$ ,  $\mathcal{P}_{\mathcal{U}}(k)$  and  $\mathcal{P}_{\mathcal{V}}(k)$  to be tiny during inflation blue for BP $a$ , BP $b$ , and BP $d$ .

Indeed, this can be seen from the fact that the square roots of the eigenvalues of the mass matrix  $\mathcal{M}_J^I + \delta\mathcal{M}_J^I$  in Eq. (30) for three modes are heavier than the Hubble scale during the inflation for each BPs, as depicted in Fig. 5. These correspond to entropy modes and this implies that fluctuations of the entropy modes are exponentially suppressed during the inflation. Also, in these kind of parameters, the valley approximations can be adopted in which, by integrating out heavy modes, and inflation dynamics can be described by a single

field-like one. Some details of the valley approximation is given in Appendix C.

On the other hand, for BP $c$ , one can see that the masses of other modes other than adiabatic one are almost the same or smaller than the Hubble scale. For parameters with light masses like BP $c$ , one generally cannot adopt the valley approximations, and one in principle has to solve all background and perturbation equations exactly. However, we explicitly checked that the isocurvature power spectra for BP $c$  are not exponentially suppressed during inflation, and still does not affect the adiabatic fluctuation significantly. Therefore even with the parameter set such as BP $c$ , we can calculate the inflationary observables in the same manner as the single-field case.

For explicit comparison we also plotted the evolution of the power spectra for the adiabatic mode  $\mathcal{P}_{\mathcal{R}}(k)$  and the entropy mode  $\mathcal{P}_{\mathcal{S}}(k)$  in Fig. 6 for all four BPs. The figure illustrates that for all BPs the power spectrum  $\mathcal{P}_{\mathcal{R}}(k)$  remains much larger than that of  $\mathcal{P}_{\mathcal{S}}(k)$ . We have checked this is also true for the  $\mathcal{P}_{\mathcal{U}}(k)$  and  $\mathcal{P}_{\mathcal{V}}(k)$ . This should be compared with the corresponding eigenvalues of the mass matrix for each BPs in Fig. 5. As mentioned above, for BP $c$ , the mass eigenvalues for isocurvature modes are not heavier than the Hubble scales, which explains the behavior that the size of  $\mathcal{P}_{\mathcal{S}}(k)$  is relatively large, although still smaller than the adiabatic one, compared to the counterpart in other BPs. However, we emphasize that even in the case of BP $c$  the effects of isocurvature modes on the adiabatic one are small enough such that the single-field description is valid. We remark that the amplification of the entropy modes such as  $\mathcal{P}_{\mathcal{S}}(k)$  at around the end of inflation can happen as can be seen in Fig. 6, which might have originated from preheating after inflation (see e.g. Refs. [94–96]). We leave a detailed analysis on this issue for future work.

Finally, we plot the spectral index  $n_s$  in Fig. 7. As the entropy perturbations are tiny, while finding Fig. 7, we simply utilize the approximate expression given for the single field inflation in Eq. (70). We find that for  $\mathcal{N} = -57.5$  and  $-57.2$  (i.e. at  $t = t_*$ ) the spectral indices for all the BPs match with the Planck 2018 observation i.e.  $n_s = 0.9649 \pm 0.0042$  at 68% CL [23] as also can be seen from Fig. 7. The Planck 2018 data also obtained the bound for the tensor-to-scalar

**Fig. 6** Evolution of the power spectrum of adiabatic mode  $\mathcal{P}_{\mathcal{R}}(k)$  and entropy mode  $\mathcal{P}_{\mathcal{S}}(k)$  for pivot scale  $k_*$  for BP*a* (upper left), BP*b* (upper right), BP*c* (lower left) and BP*d* (lower right) respectively

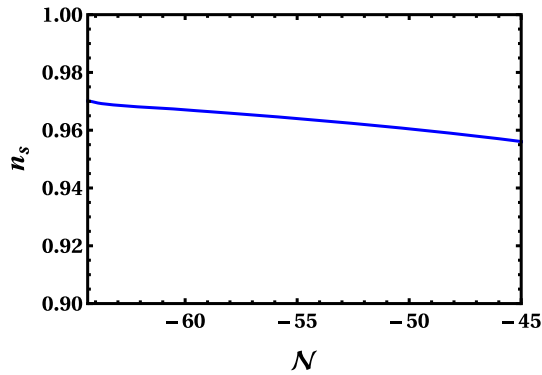
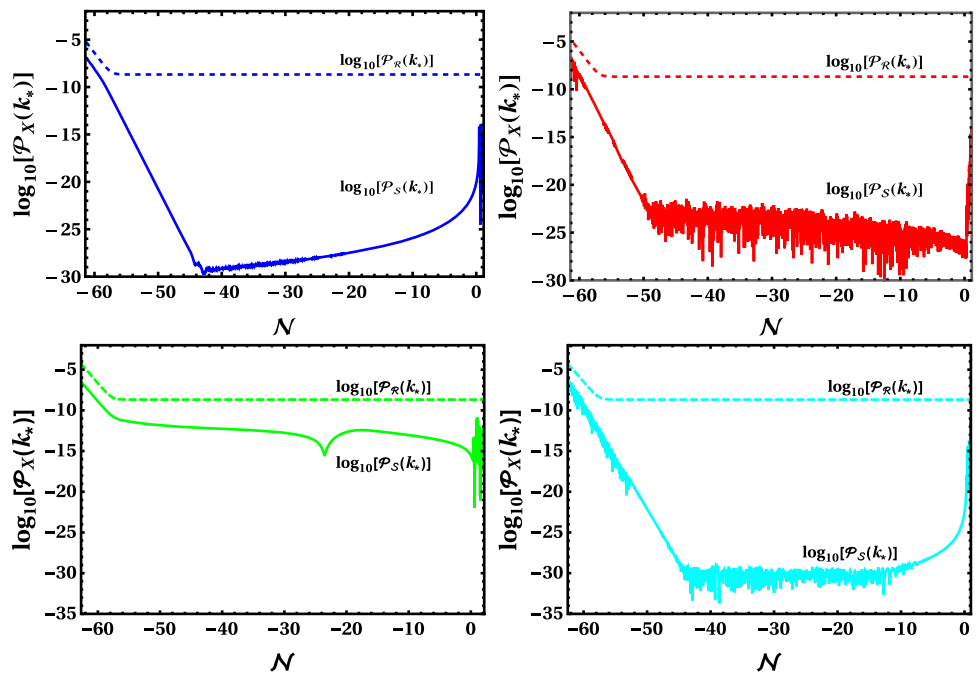


**Fig. 7** The  $n_{\mathcal{R}}$  vs  $\mathcal{N}$  plot as in Eq. (70) for BP*a*

ratio as  $r < 0.056$  [23]. By including the BICEP/Keck 2018 data, the constraint became tighter as  $r < 0.036$  [97].

We find  $r \approx 3.35 \times 10^{-3}$  and  $\approx 3.37 \times 10^{-3}$  for the respective BPs, which is well below the current observational bounds, but can be detectable future CMB B-mode experiments such as LiteBIRD [98] and the Simons Observatory [99]. Although we do not discuss in detail and provide any figures for other PBs, we have checked that the other cases almost give similar values for  $n_s$  and  $r$ .

### 5 Implications for collider experiments

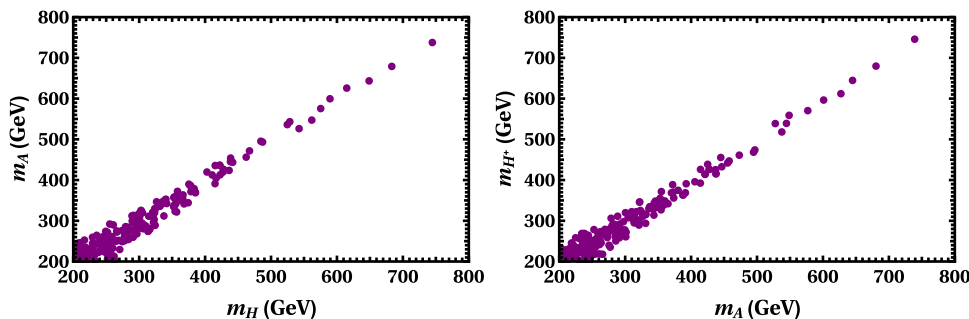
Let us discuss implications of the  $R^2$ -Higgs inflation for collider experiments. For illustration, in Sect. 4, we have chosen benchmark points for our analysis. Notwithstanding, there exists larger sub-TeV parameter space for H, A and  $H^\pm$  that can account for  $R^2$ -Higgs inflation in the g2HDM. In Fig. 8

we provide scanned parameter space for  $m_A$ ,  $m_H$  and  $m_{H^\pm}$  that can provide successful  $R^2$ -Higgs inflation satisfying all inflationary conditions and observational constraints from Planck 2018 [23].

As can be seen from Fig. 8 for the successful  $R^2$ -Higgs inflation quasi-degenerate mass spectrum is required for the heavy Higgs bosons  $m_H$ ,  $m_A$  and  $m_{H^\pm}$ . This finding is similar to Higgs inflation in g2HDM but without the  $R^2$  term [50]. This is primarily due to the requirement of perturbativity for the  $\tilde{\eta}_i$  for inflationary dynamics at high scale. We find that parameter points with  $\eta_i > 1$  at low scale (i.e.  $y = 0$ ) grow too large at high scale and get excluded by the perturbativity requirements. Due to limited computational facility for scanning we restricted all  $\eta_i$  at low scale to be  $< 1$ . With a common  $\mu_{22}^2$  terms, the  $m_H$ ,  $m_A$  and  $m_{H^\pm}$  mass degeneracy gets practically restricted due to these small values of  $\eta_i$  at low scale which can be seen easily from Eqs. (3)–(5). This has unique implications for collider experiments, that is, a future discovery of quasi-degenerate  $m_H$ ,  $m_A$  and  $m_{H^\pm}$  would provide a smoking gun signature for  $R^2$ -Higgs inflation in the g2HDM.

While the Yukawa couplings  $\rho_{ij}^F$  do not play significant role in the inflationary dynamics and only enter in the  $\beta$  functions of the quartic couplings  $\eta_i$ s, however, they could play important role in the discovery and/or constraining the parameter space for H, A and  $H^\pm$ . Here we assumed  $\rho_{ii}^F \sim \lambda_i^F$  with suppressed off diagonal elements for the  $\rho_{ij}^F$  matrices. In particular, we assumed extra Yukawa couplings  $\rho_{tt}^U = 0.5$  and  $\rho_{tc}^U = 0.2$  for the RG running for all the BPs discussed in the previous section and turned off other extra Yukawa couplings for simplicity. In what follows we shall see that for these values of extra Yukawa couplings are allowed by

**Fig. 8** The scanned parameter space in the  $m_A$ - $m_H$  (left) and  $m_A$ - $m_{H^\pm}$  (right) plane that can provide successful  $R^2$ -Higgs inflation



direct and indirect searches and may lead to discovery of the heavy Higgs bosons.

### 5.1 Indirect searches

First we focus on the coupling measurements  $h$  boson at the LHC. A nonvanishing  $c_\gamma$  can alter the couplings of 125 GeV  $h$  boson e.g. to fermions, as can be seen from Eq. (6). Following the prescription given in Ref. [100] we find that  $|\rho_{tt}^U| = 0.5$  is well allowed at  $2\sigma$  by the current measurements of top Yukawa coupling of  $h$  by ATLAS [101] and CMS [102] with full Run 2 data. The limit is rather weak primarily due to the small  $c_\gamma$  values (see Table 2) for all the BPs. We remark that such coupling measurements in general allows  $\rho_{tt}^U \sim 0.5$  if  $c_\gamma \lesssim 0.1$ .

The  $\rho_{tt}^U$  also receives stringent constraints from flavor physics, e.g. nonvanishing  $\rho_{tt}^U$  enters in  $B_{s,d}$  mixing amplitude as well as branching ratio of  $B \rightarrow X_s \gamma$  ( $\mathcal{B}(B \rightarrow X_s \gamma)$ ) at one loop through  $t b H^\pm$  vertex [103]. The strongest limit arises however from the  $B_{s,d}$  mixing. Allowing  $2\sigma$  error on the UTfit results for  $B_{s,d}$  [104] and following the expression given in Ref. [103], we find that  $|\rho_{tt}^U| \lesssim 0.5$  is allowed at  $2\sigma$  for all the BPs. This suggest that for the ballpark value of  $\rho_{tt}^U$  assumed here, flavor physics already provides indirect probe for the inflationary dynamics in particular for  $m_{H^\pm} \sim 200$ –600 GeV, but the constraint becomes milder for heavier  $m_{H^\pm}$ . In this regard future LHCb [105] and Belle-II [106] measurements would offer a further stringent test for the sub-TeV  $m_{H^\pm}$  if  $\rho_{tt}^U$  is not vanishingly small.

The flavor changing coupling  $\rho_{tc}^U$  does not enter  $h$  boson couplings at tree level however it may induce top flavor changing decay  $t \rightarrow ch$  if  $c_\gamma$  is nonzero. Such searches are performed and strong upper limits on the branching ratios of  $t \rightarrow ch$  ( $\mathcal{B}(t \rightarrow ch)$ ) are already set by both ATLAS [107] and CMS [108]. We find that the CMS 95% CL upper limit  $\mathcal{B}(t \rightarrow ch) < 7.3 \times 10^{-4}$  [108] is mildly stronger than the ATLAS one. Utilizing these limits it has been found that  $\rho_{tc}^U \lesssim 0.75$  is still allowed at 95% CL if  $c_\gamma = 0.1$  [109]. This means that our chosen value  $\rho_{tc}^U = 0.2$  is well allowed by data. There also exist constraints on  $\rho_{tc}^U$  from flavor physics. Relevant constraints arise also from  $\mathcal{B}(B \rightarrow X_s \gamma)$  where  $\rho_{tc}^U$  enters via charm loop through  $H^+$  coupling [103]. Reinterpreting results from Ref. [110] we find that  $\rho_{tc}^U \gtrsim 1$  is

excluded at  $2\sigma$  if  $m_{H^\pm} \sim 200$ –500 GeV. We remark that the constraint is weak and becomes even milder for heavier  $m_{H^\pm}$ .

In general other  $\rho_{ij}^F$  couplings such as  $\rho_{bb}^D$  and  $\rho_{tt}^U$  could still be large, e.g., extra Yukawa couplings  $|\rho_{bb}^D| \lesssim 0.1$ –0.15 is still allowed by current data for  $m_H, m_A, m_{H^\pm} \in [200, 800]$  GeV [87, 89, 111]. Furthermore, we also remark that there also exist some indirect measurements that provide some constraints on  $\rho_{tt}^U$ . E.g.,  $B \rightarrow \mu\nu$  and  $D$ -meson mixing provide some constraints but still allow  $\rho_{tt}^U \sim 0.1$ –0.2 at  $2\sigma$  level [112, 113]. If they are nonvanishing they may offer additional probes for the parameter space required for  $R^2$ -Higgs inflation in the g2HDM.

### 5.2 Direct searches

Nonzero  $\rho_{tt}^U$  can induce  $V_{tb}$  enhanced  $bg \rightarrow tH^+$  and  $gg \rightarrow t\bar{b}H^+$  processes (charge conjugate processes are implied). The processes  $pp \rightarrow t(b)H^+$  followed by  $H^+ \rightarrow t\bar{b}$  are the conventional search program for the  $H^\pm$  of ATLAS [114] and CMS [115]. Further for  $m_A/m_H > 2m_t$ ,  $\rho_{tt}^U$  coupling can initiate  $gg \rightarrow H/A \rightarrow t\bar{t}$ , which are already being searched by ATLAS [116] and CMS [117]. In general, such searches exclude  $\rho_{tt}^U \gtrsim 0.6$ –1 at 95% CL for  $m_H, m_A, m_{H^\pm} \in [200, 800]$  GeV [118].

There also exist direct searches that can constrain the flavor changing coupling  $\rho_{tc}^U$ . The most relevant search in this regard is CMS search for SM four-top production [119]. It has been found [86, 120] that  $\rho_{tc}^U$  coupling induced  $cg \rightarrow tH/tA \rightarrow t\bar{t}c$  processes contribute abundantly to the control region of  $t\bar{t}W$  background of the CMS search which excludes  $|\rho_{tc}^U| \lesssim 0.4$ –0.6 in the  $m_H, m_A \in [200, 600]$  GeV [86, 88, 109, 118, 120–124]. As our working assumption was  $\rho_{ii}^F \sim \lambda_i^F$  and suppressed off-diagonal elements, in general couplings such as  $\rho_{bb}^D$  and  $\rho_{\tau\tau}^L$  are below the sensitivity of the LHC.

### 5.3 Probing the quasi-degeneracy

The processes mentioned above together may allow discovery of the heavy Higgs bosons  $H, H^\pm$  and  $A$ , however, one could only attribute a parameter space in the g2HDM to the  $R^2$ -Higgs inflation if quasi-degeneracy is also observed. This

would require tricky reconstruction of the masses of these heavy Higgs bosons or finding out processes that are sensitive to mass degeneracies. In this subsection we discuss how to probe such quasi-degeneracy in LHC or future lepton colliders.

For nonvanishing  $\rho_{tt}$  the  $H^\pm$  can be reconstructed in the sub-TeV range via  $bg \rightarrow \bar{i}(b)H^+$  followed by  $H^+ \rightarrow t\bar{b}$  decay as already discussed by ATLAS [114] and CMS [115]. In general reconstruction might be also possible e.g. via process such as  $gg \rightarrow H/A \rightarrow t\bar{t}$  if  $m_A/m_H > 2m_t$ . The searches performed so far by ATLAS [116] and CMS [117] assume decoupled  $m_A$  and  $m_H$ . Therefore while discovery is possible, however, extraction of information on quasi-degeneracy would be particularly difficult due to interference between  $gg \rightarrow A \rightarrow t\bar{t}$ ,  $gg \rightarrow H \rightarrow t\bar{t}$  and SM  $gg \rightarrow t\bar{t}$ . For nonvanishing  $\rho_{tc}^U$  and  $\rho_{tt}^U$  one may have discovery via  $gg \rightarrow H/A \rightarrow t\bar{c}$  [103], however the interference between  $gg \rightarrow A \rightarrow t\bar{c}$  and  $gg \rightarrow H \rightarrow t\bar{c}$  would again obscure the information on mass degeneracy. Additionally one may have discovery via  $cg \rightarrow tH/tA \rightarrow t\bar{t}$  [122] or  $cg \rightarrow bH^+ \rightarrow bt\bar{b}$  [118] at the high-luminosity LHC if both  $\rho_{tc}^U$  and  $\rho_{tt}^U$  are nonzero.

It is clear that to probe quasi-degeneracy of  $H$  and  $A$  one requires careful analysis due to multiple interfering contributions. In such scenarios we propose to study  $cg \rightarrow tH/tA \rightarrow t\bar{t}\bar{c}$  (denoted as same-sign top) at the LHC which may provide *smoking gun* signature for the quasi-degeneracy between  $H$  and  $A$ . It has been found that if  $H$  and  $A$  are both mass and width degenerate the process  $cg \rightarrow tH \rightarrow t\bar{t}\bar{c}$  and  $cg \rightarrow tA \rightarrow t\bar{t}\bar{c}$  cancel each other exactly due to destructive interference [122]. This is primarily due to the amplitude for  $cg \rightarrow tA \rightarrow t\bar{t}\bar{c}$  picks up a factor of  $i^2\gamma_5$  compared to  $cg \rightarrow tH \rightarrow t\bar{t}\bar{c}$ , as can be seen from Eq. (6). The cancellation diminishes if the mass and/or widths become non-degenerate.

Let us briefly discuss the potential of the same-sign top signature to probe quasi-degeneracy between  $H$  and  $A$ . For illustration we consider BP $a$  and BP $c$ . Moreover, we assume  $\rho_{tt}^U = 0.5$  and  $\rho_{tc}^U = 0.5$  which we have checked are allowed by all direct and indirect searches mentioned above. We turn off all other  $\rho_{ij}$  couplings, however shall return to their impact on mass reconstruction at the end of this section. Under the above mentioned assumptions the total decay widths for  $A$  ( $H$ ) are sum of partial rates of  $A \rightarrow t\bar{c} + \bar{t}c$  ( $H \rightarrow t\bar{c} + \bar{t}c$ ) and,  $A \rightarrow \bar{t}t$  ( $H \rightarrow \bar{t}t$ ) for BP $a$ . But for BP $c$  both  $A$  and  $H$  decays practically 100% to  $t\bar{c} + \bar{t}c$ . For  $\rho_{tt}^U = 0.5$  and  $\rho_{tc}^U = 0.5$  we find the decay widths of  $A$  and  $H$  are 2.43 (8.58) and 2.41 (6.04) GeV for BP $c$  (BP $a$ ).

The same-sign top can be searched at LHC via  $pp \rightarrow tH/tA + X \rightarrow t\bar{t}\bar{c} + X$  with both the top quarks decaying semileptonically comprising same-sign dilepton ( $ee, e\mu, \mu\mu$ ) plus at least three jets with at least two  $b$ -tagged and one non- $b$ -tagged, and missing energy ( $E_T^{\text{miss}}$ )

The SM backgrounds for the process are  $t\bar{t}Z, t\bar{t}W, 4t, t\bar{t}h$  and  $tZ$  + jets. Additionally, for the same-sign top signature the SM  $t\bar{t}$  and  $Z/\gamma^* + \text{jets}$  processes would contribute if one of the lepton charge is misidentified ( $Q$ -flip). Notwithstanding, it has been found that the non-prompt background could be  $\sim 1.5$  times of the  $t\bar{t}W$  background for the same-sign top signature [122].

In order to demonstrate the discovery potential we generate the signal and background events at  $\sqrt{s} = 14$  TeV via MadGraph5\_aMC@NLO [125] with the parton distribution function (PDF) set NN23LO1 [126]. The events are then interfaced with PYTHIA 6.4 [127] for showering and hadronization, and then fed into Delphes 3.4.2 [128] to incorporate detector effects (ATLAS based).

To suppress backgrounds and optimize for the same-sign top signature we apply following event selection cuts. The leading and subleading lepton transverse momenta  $p_T$  should be  $> 25$  and  $> 20$  GeV respectively, while the pseudo-rapidity  $|\eta| < 2.5$ . For all three jets we require  $p_T > 20$  GeV and also  $|\eta| < 2.5$ , and  $E_T^{\text{miss}} > 30$  GeV. The separation  $\Delta R$  between any jets and a lepton ( $\Delta R_{\ell j}$ ), the two  $b$ -jets ( $\Delta R_{bb}$ ), and any two leptons ( $\Delta R_{\ell\ell}$ ) should be  $\Delta R > 0.4$ . Finally, we impose  $H_T$  i.e. the sum of the  $p_T$  of the two leading leptons included and two leading  $b$ -jets and the leading non  $b$ -tagged jets should  $> 300$  GeV.

The background cross sections after the application of the above selection cuts are summarized in Table 3 while the signal cross sections for the reference mass scenario BP $a$  (BP $c$ ) is 0.023 (0.18) fb. The corresponding statistical significances are  $\sim 1\sigma$  and  $\sim 4\sigma$  respectively with  $3000 \text{ fb}^{-1}$  luminosity; which are estimated by using  $\mathcal{Z} = \sqrt{2[(S+B)\ln(1+S/B) - S]}$  [129], where the  $S$  and  $B$  are the number of signal and background events after selection cuts. This simply illustrates that discovery of same-sign top process is not possible for both the scenarios even at the high luminosity LHC (HL-LHC). In general, same-sign top signature for these reference mass ranges are expected to be discovered much earlier than full HL-LHC data for  $\rho_{tt}^U = 0.5$  and  $\rho_{tc}^U = 0.5$  if  $H$  and  $A$  are degenerate [122]. Hence, discoveries of  $gg \rightarrow H/A \rightarrow t\bar{t}$ ,  $cg \rightarrow tH/tA \rightarrow t\bar{t}$  and  $cg \rightarrow bH^+ \rightarrow bt\bar{b}$  and non-observation or milder significance of the same-sign top in the HL-LHC era may indicate quasi-degeneracy of  $H$  and  $A$  whereas, the charged Higgs mass can be reconstructed via  $bg \rightarrow \bar{i}(b)H^+ \rightarrow \bar{i}(b)t\bar{b}$ .

Probing the quasi-degeneracy at the LHC becomes particularly challenging if  $\rho_{tc}^U$  or  $\rho_{tt}^U$  are small. Furthermore, processes such as  $gg \rightarrow H/A \rightarrow t\bar{t}$  and  $cg \rightarrow tH/tA \rightarrow t\bar{t}$  are only sensitive above  $m_A/m_H > 2m_t$  threshold. In such cases  $e^+e^-$  colliders such as ILC or FCC- $ee$  could be useful for discovery and, possibly even for probing quasi-degeneracy. In this regard we propose to study  $e^+e^- \rightarrow Z^* \rightarrow AH$ ,  $e^+e^- \rightarrow Z^*/\gamma \rightarrow H^+H^-$ ,  $e^+e^- \rightarrow Z^* \rightarrow Ah$  followed by  $A/H \rightarrow t\bar{c} + \bar{t}c/t\bar{t}$  or  $H^+ \rightarrow c\bar{b}/t\bar{b}$ . Depending on the



**Table 3** The background cross sections after selection cuts for the same-sign top search. The backgrounds cross sections are all normalized to either NLO or NNLO as in Ref. [122]

Backgrounds	Cross section (fb)
$t\bar{t}W$	1.31
$t\bar{t}Z$	1.97
$4t$	0.316
$tZ$ +jets	0.255
$t\bar{t}h$	0.07
$Q$ -flip	0.024
Nonprompt	$1.5 \times t\bar{t}W$

values of  $\rho_{tc}^U$  or  $\rho_{tt}^U$ , these processes may require  $\geq 1$  TeV CM energy and/or high-luminosity  $e^+e^-$  collider for discovery, while probing the quasi-degeneracy of  $H$  and  $A$ ,  $H^\pm$  would perhaps require even higher statistics.

So far we have turned off other  $\rho_{ij}$  couplings for simplicity. In general  $\rho_{bb}^D$  could be nonvanishing and would open up new modes for mass reconstruction such as  $bg \rightarrow bA \rightarrow bZh$  process at the LHC or at future lepton collider via  $e^+e^- \rightarrow Z^* \rightarrow AH$ , followed by  $A(H) \rightarrow b\bar{b}$  decay. For nonzero  $\rho_{\tau\tau}^L$  discovery is possible via  $gg \rightarrow H/A \rightarrow \tau^+\tau^-$  at the LHC or  $gb \rightarrow tH^+ \rightarrow t\tau^+\nu_\tau$  processes. For finite discussion, we however do not turn on all these  $\rho_{ij}$  couplings together since they would initiate many new direct and indirect signatures that are not discussed here. Such scenario would nonetheless be interesting and require a more dedicated analysis which is beyond the scope of the current paper.

## 6 Discussion and summary

We have studied  $R^2$ -Higgs inflation in the g2HDM where the inflationary dynamics consists of four fields  $\varphi$ ,  $\rho_1$ ,  $\rho_2$  and  $\rho_3$  using the covariant formalism. We first discussed relevant background dynamics and perturbation theory for the field fluctuations for our four field model. We found that, by numerically solving the set of equations for the background and perturbation evolutions, primordial power spectra for the parameter sets consistent with Planck observations [23] and low energy constraints can be well described by a single-field approximation where the field  $\varphi$  nearly plays the role of inflaton, whereas  $\rho_1$ ,  $\rho_2$  and  $\rho_3$  play isocurvature fields during inflation and those isocurvature modes scarcely affect the adiabatic one by appropriately choosing the initial values for isocurvature fields. However, we note that there may exist parameter space where the entropy modes affect the power spectrum for the adiabatic one and/or primordial non-Gaussianities. This shall be studied elsewhere.

Throughout the paper we have just turned on one nonminimal couplings  $\xi_{11}$  for simplicity. In general the nonminimal couplings  $\xi_{12}$  and  $\xi_{22}$  can also drive inflation as discussed in Ref. [50]. In the 2HDM inflation without the  $R^2$  term, the inflationary dynamics for the nonminimal couplings  $\xi_{22}$  (and  $\xi_{12}$ ) is quite similar to that of  $\xi_{11}$  [50]. However, a similar conclusion can not be drawn here. As the parameterization of Eq. (9) of the current article is different than the one in Ref. [50] the different  $\xi_{ij}$  couplings may have very distinct inflationary dynamics. While it would indeed be interesting to see the impacts of these nonminimal couplings individually or, when they are turned on together, however, we leave out a detailed analysis on this for future.

For illustration we chose four benchmark points for our analysis with  $m_H$ ,  $m_A$  and  $m_{H^\pm} \sim 400$  GeV. To satisfy the normalization to CMB power spectrum [23], in the  $R^2$ -like BP  $a$  and  $c$  we have assumed the scalaron self couplings  $\xi_R$  to be large. In the mixed  $R^2$ -Higgs like BP  $b$  and  $d$  the normalization to CMB data is achieved by considering both  $\xi_R$  and nonminimal coupling  $\xi_{11}$  to be relatively large. For all the BPs, the predicted spectral index  $n_s$  and tensor-to-scalar ratio  $r$  are within their experimental bounds [23].

Although for all the benchmark points we considered  $m_H$ ,  $m_A$  and  $m_{H^\pm} \sim 400$  GeV, there exists parameter space for a successful inflationary scenario in the sub-TeV range i.e.  $m_H$ ,  $m_A$  and  $m_{H^\pm} \in [200, 800]$  GeV, as found in Ref. [50]. This mass range has a unique impact for the ongoing collider experiments such as the LHC(b) and Belle-II. We discussed a discovery scope for these bosons at the upcoming LHC run and, plausible indirect probes at the flavor machines such as LHCb and Belle-II. A discovery of these additional bosons along with the confirmation of their quasi-degeneracy may hint the g2HDM as a likely mechanism for the cosmic inflation. Here we also remark that we have assumed all  $\rho_{ij}^F$  couplings to be real. In general, along with the quartic couplings  $\eta_{5,6,7}$  they can be complex in nature. The implications of such complex couplings during (and after) inflation including baryogenesis are yet to be analyzed in the g2HDM. (See Ref. [130] for a baryogenesis scenario during the reheating in Higgs inflation.) However, they are already within the reach [89] of CP sensitive measurements such as electron electric dipole moment of ACME collaboration [131] and the CP asymmetry for  $B \rightarrow X_s \gamma$  decay at Belle [132].

We also further remark on the unitarity problem of the 2HDM inflation model. The cut-off scale for 2HDM inflation at low field regime is given by  $\min(M_P/\xi_{ij})$  with  $i, j = 1, 2$  [51]. As already mentioned in the introduction, inflationary dynamics with large field values does not suffer the unitarity violation due to field-dependent cut-off. However, it is known that the issue of unitarity arises again during the preheating stages since the produced particles have energy larger than the cut-off scale due to the existence of the large non-minimal coupling [28–30]. Even though a detailed study of the reheat-



ing in 2HDM inflation is not the scope of the current paper, it is reasonable to think that there may be a similar issue in the 2HDM inflation without the  $R^2$  term; this is because the violent preheating is a generic feature of large non-minimal coupling. (However, see also Ref. [133]) A more complete discussion of the unitarity violation of 2HDM inflaton will be further studied elsewhere. Moreover, we remark that regardless of the unitarity violation, if one wants to have a theory valid up to Planck scale for entire field range,  $R^2$ -2HDM inflation perhaps can be considered as a UV completion of the model as well.

One key implications of  $R^2$ -Higgs inflation in the g2HDM is quasi-degenerate mass spectrum for H, A and  $H^\pm$ . Without the confirmation of such quasi-degeneracy, a discovery of heavy Higgs bosons may not be sufficient to make a connection to the inflationary scenario. Depending on the magnitude of the additional Yukawa couplings  $\rho_{tt}^U, \rho_{tc}^U, \rho_{bb}^D$  etc. such mass reconstruction may be partially possible at the LHC in certain scenarios, however, one may need future electron-positron collider such as ILC or FCCee.

**Acknowledgements** The work of SML was supported in part by the National Research Foundation of Korea (NRF) grant funded by the Korea government (MOE) (no. 2020R1A6A3A13076216). SML is also supported by the Hyundai Motor Chung Mong-Koo Foundation Scholarship. The work of TM is supported by a Postdoctoral Research Fellowship from the Alexander von Humboldt Foundation. The work of KO is in part supported by KAKENHI Grant nos. 19H01899 and 21H01107. The work of TT is supported in part by JSPS KAKENHI Grant numbers 17H01131, 19K03874 and MEXT KAKENHI Grant number 19H05110.

**Data Availability Statement** This manuscript has no associated data or the data will not be deposited. [Authors' comment: This is a theoretical work. There is no associated data.]

**Open Access** This article is licensed under a Creative Commons Attribution 4.0 International License, which permits use, sharing, adaptation, distribution and reproduction in any medium or format, as long as you give appropriate credit to the original author(s) and the source, provide a link to the Creative Commons licence, and indicate if changes were made. The images or other third party material in this article are included in the article's Creative Commons licence, unless indicated otherwise in a credit line to the material. If material is not included in the article's Creative Commons licence and your intended use is not permitted by statutory regulation or exceeds the permitted use, you will need to obtain permission directly from the copyright holder. To view a copy of this licence, visit <http://creativecommons.org/licenses/by/4.0/>.  
Funded by SCOAP<sup>3</sup>.

**Appendix A: Field space metric and Christoffel symbols**

The nonvanishing Christoffel symbols (with  $M_P = 1$ ) are

$$\Gamma_{\phi_2\phi_2}^{\phi_1} = \Gamma_{\phi_3\phi_3}^{\phi_1} = \Gamma_{\phi_4\phi_4}^{\phi_1} = \frac{e^{-\sqrt{\frac{2}{3}}\varphi}}{\sqrt{6}}$$

$$\begin{aligned} \Gamma_{\phi_1\phi_2}^{\phi_2} &= \Gamma_{\phi_1\phi_2}^{\phi_2} = -\frac{1}{\sqrt{6}}, \\ \Gamma_{\phi_1\phi_3}^{\phi_3} &= \Gamma_{\phi_3\phi_1}^{\phi_3} = -\frac{1}{\sqrt{6}}, \\ \Gamma_{\phi_1\phi_4}^{\phi_4} &= \Gamma_{\phi_4\phi_1}^{\phi_4} = -\frac{1}{\sqrt{6}}. \end{aligned} \tag{A.1}$$

**Appendix B: The approximate initial conditions**

Let us perform following field redefinition [51]:

$$\begin{aligned} \rho &= \frac{\sqrt{\rho_2^2 + \rho_3^2}}{\rho_1}, \quad \tau = \frac{s}{\rho_1^2}, \quad c_\chi = \frac{\rho_2}{\sqrt{\rho_2^2 + \rho_3^2}} \\ \varphi &= \sqrt{\frac{3}{2}} M_P \ln(F^2) \end{aligned} \tag{B.2}$$

where we have used shorthand notation  $\cos \chi = c_\chi$ . The conformal factor becomes

$$\frac{1}{F^2} = \frac{M_P^2 \left(1 - e^{-\sqrt{\frac{2}{3}}\frac{\varphi}{M_P}}\right)}{\xi_{11}\rho_1^2 + \xi_R s}. \tag{B.3}$$

The potential  $V_E$  in Eq. (13) can now be expressed in terms of  $(\varphi, \rho, \chi, \tau)$  as

$$\begin{aligned} V_E(\varphi, \rho, \tau, \chi) &= \frac{M_P^4 (\eta_{\text{eff}} + 2\xi_R \tau^2)}{8(\xi_{11} + \xi_R \tau)^2} \\ &\times \left(1 - e^{-\sqrt{\frac{2}{3}}\frac{\varphi}{M_P}}\right)^2. \end{aligned} \tag{B.4}$$

with

$$\begin{aligned} \eta_{\text{eff}} &= \tilde{\eta}_1 + \tilde{\eta}_2 \rho^4 + 2\rho^2(\tilde{\eta}_3 + \tilde{\eta}_4 + (2c_\chi^2 - 1)\tilde{\eta}_5) \\ &+ 4c_\chi \rho (\tilde{\eta}_6 + \tilde{\eta}_7 \rho^2). \end{aligned} \tag{B.5}$$

The potential in Eq. (B.4) is now in the single field attractor form with  $\varphi$  playing the role of the inflaton once it is minimized with respect to  $\rho, \tau$  and  $c_\chi$ . Here for sake of simplicity we minimize first  $\eta_{\text{eff}}$  with respect to  $\rho$  and  $\chi$ . This is essentially minimizing the potential  $V$  in the  $\rho$  and  $c_\chi$  direction as discussed in the context of Higgs inflation in 2HDM in Ref. [50]. We follow the same numerical minimization procedure as in Ref. [50]. The  $\eta_{\text{eff}}$  has a extremum at  $(\rho_0, c_{\chi_0})$ , which is found by solving  $\partial V/\partial \rho = 0$  and  $\partial V/\partial c_\chi = 0$  simultaneously. The extremum is considered a minimum if both the determinant and trace of the covariant matrix  $X_{ij} = \partial^2 V/\partial x_i \partial x_j$  (with  $x_{i,j} = \rho$  and  $c_\chi$ ), calcu-

lated at the minima  $(\rho_0, c_{\chi_0})$ , are  $> 0$ . We find the  $\eta_{\text{eff}}^{\text{min}}$  as

$$\eta_{\text{eff}}^{\text{min}} = \tilde{\eta}_1 + \tilde{\eta}_2 \rho_0^4 + 2\rho_0^2 (\tilde{\eta}_3 + \tilde{\eta}_4 + (2c_{\chi_0}^2 - 1)\tilde{\eta}_5) + 4c_{\chi_0} \rho_0 (\tilde{\eta}_6 + \tilde{\eta}_7 \rho_0^2). \tag{B.6}$$

One can now insert  $\eta_{\text{eff}}^{\text{min}}$  in Eq. (B.4) and minimize with respect to  $\tau$  where the minimum is found as

$$\tau_0 = \eta_{\text{eff}}^{\text{min}} / (2\xi_{11}). \tag{B.7}$$

Substituting  $\tau_0$  we find

$$V_E = \frac{M_P^4}{4} \frac{1}{\left(\frac{2\xi_{11}^2}{\eta_{\text{eff}}^{\text{min}}} + \xi_R\right)} \left(1 - e^{-\sqrt{\frac{2}{3}} \frac{\varphi}{M_P}}\right)^2. \tag{B.8}$$

We can now utilize Eq. (B.8) to find the  $\varphi$  value that would satisfy the Planck 2018 measurements once the kinetic terms are canonically normalized. We do not perform slow roll approximation, however, follow the covariant formalism and solve background field equations Eq. (29) with the initial conditions of  $\varphi, \rho_1, \rho_2$  and  $\rho_3$  being simply translated from these minimized values of  $\rho, c_\chi$  and  $\tau$  and  $\varphi$  via Eq. (B.2). Here we stress the all four fields  $\varphi, \rho_1, \rho_2$  and  $\rho_3$  start at the top of the ridge with these initial conditions but they quickly settles to the trajectories such that  $\varphi$  essentially plays the role of inflaton.

### Appendix C: Valley approximations

When there is a well-defined trajectory of the inflaton with valley shaped potential, we have single field-like behavior and  $\rho_i (i = 1, 2, 3)$  fields can be represented as a function of  $\varphi$ . In this Appendix, we present analytic understanding of these approximations.

The potential in the Einstein frame is given by

$$V_E(\varphi, \rho_1, \rho_2, \rho_3) = \frac{1}{8} e^{-2\sqrt{\frac{2}{3}} \frac{\varphi}{M_P}} \left[ V(\rho_1, \rho_2, \rho_3) + 2 \frac{M_P^4}{\xi_R} \left( e^{\sqrt{\frac{2}{3}} \frac{\varphi}{M_P}} - 1 - \frac{\xi_{11}}{M_P^2} \rho_1^2 \right)^2 \right], \tag{C.9}$$

with

$$V(\rho_1, \rho_2, \rho_3) = \eta_1 \rho_1^4 + \eta_2 (\rho_2^2 + \rho_3^2)^2 + 2\eta_5 (\rho_2^2 - \rho_3^2) \rho_1^2 + 2(\eta_3 + \eta_4) (\rho_2^2 + \rho_3^2) \rho_1^2 + 4\rho_2 \rho_1 \times \left\{ \eta_6 \rho_1^2 + \eta_7 (\rho_2^2 + \rho_3^2) \right\} \tag{C.10}$$

where we did not explicitly put tildes for  $\eta$ s. From this, we have the following set of equations for the valley:

$$\frac{\partial V_E}{\partial \rho_1} / \left( \frac{1}{2} e^{-2\sqrt{\frac{2}{3}} \varphi} \right) = \eta_1 \rho_1^3 + 2 \frac{\xi_{11}}{\xi_R} \rho_1 \left( 1 - e^{\sqrt{\frac{2}{3}} \varphi} + \xi_{11} \rho_1^2 \right) + 3\eta_6 \rho_1^2 \rho_2 + \eta_5 \rho_1 (\rho_2 - \rho_3) (\rho_2 + \rho_3) + (\eta_3 + \eta_4) \rho_1 (\rho_2^2 + \rho_3^2) + \eta_7 \rho_2 (\rho_2^2 + \rho_3^2) = 0, \tag{C.11}$$

$$\frac{\partial V_E}{\partial \rho_2} / \left( \frac{1}{2} e^{-2\sqrt{\frac{2}{3}} \varphi} \right) = \eta_6 \rho_1^3 + \rho_2 [(\eta_3 + \eta_4 + \eta_5) \rho_1^2 + 3\eta_7 \rho_1 \rho_2 + \eta_2 \rho_2^2] + (\eta_7 \rho_1 + \eta_2 \rho_2) \rho_3^2 = 0, \tag{C.12}$$

$$\frac{\partial V_E}{\partial \rho_3} / \left( \frac{1}{2} e^{-2\sqrt{\frac{2}{3}} \varphi} \right) = \rho_3 [(\eta_3 + \eta_4 - \eta_5) \rho_1^2 + 2\eta_7 \rho_1 \rho_2 + \eta_2 \rho_2^2 + \eta_2 \rho_3^2] = 0. \tag{C.13}$$

From the last equation Eq. (C.13), we have  $\rho_3 = 0$ .

Then Eq. (C.12) reduces to

$$\eta_2 x^3 + 3\eta_7 x^2 + (\eta_3 + \eta_4 + \eta_5)x + \eta_6 = 0, \tag{C.14}$$

where  $x \equiv \frac{\rho_2}{\rho_1}$ . For our parameters, we have one real solution, which is denoted by  $x = C$ . Then we have  $\rho_2 = C\rho_1$ . Finally, by having  $\rho_3 = 0$  and  $\rho_2 = C\rho_1$ , Eq. (C.11) gives

$$\rho_1 = D \sqrt{e^{\sqrt{\frac{2}{3}} \varphi} - 1} \quad \text{with,} \\ D \equiv \frac{\sqrt{2\xi_{11}}}{\sqrt{\xi_R(C^3 \eta_7 + C^2(\eta_3 + \eta_4 + \eta_5) + 3C\eta_6 + \eta_1) + 2\xi_{11}^2}}. \tag{C.15}$$

### References

1. A.A. Starobinsky, Phys. Lett. B **91**, 99–102 (1980)
2. K. Sato, Mon. Not. R. Astron. Soc. **195**, 467–479 (1981). NORDITA-80-29
3. A.H. Guth, Phys. Rev. D **23**, 347–356 (1981)
4. V.F. Mukhanov, G.V. Chibisov, JETP Lett. **33**, 532–535 (1981)
5. A.A. Starobinsky, Phys. Lett. B **117**, 175–178 (1982)
6. S.W. Hawking, Phys. Lett. B **115**, 295 (1982)
7. A.H. Guth, S.-Y. Pi, Phys. Rev. Lett. **49**, 1110–1113 (1982)
8. F.L. Bezrukov, M. Shaposhnikov, Phys. Lett. B **659**, 703–706 (2008)
9. A.O. Barvinsky, A.Y. Kamenshchik, A.A. Starobinsky, JCAP **11**, 021 (2008)
10. F. Bezrukov, A. Magnin, M. Shaposhnikov, S. Sibiryakov, JHEP **01**, 016 (2011)
11. F. Bezrukov, Class. Quantum Gravity **30**, 214001 (2013)
12. A. De Simone, M.P. Hertzberg, F. Wilczek, Phys. Lett. B **678**, 1–8 (2009)
13. F.L. Bezrukov, A. Magnin, M. Shaposhnikov, Phys. Lett. B **675**, 88–92 (2009)
14. A.O. Barvinsky, A.Y. Kamenshchik, C. Kiefer, A.A. Starobinsky, C.F. Steinwachs, Eur. Phys. J. C **72**, 2219 (2012)
15. B.L. Spokoiny, Phys. Lett. B **147**, 39–43 (1984)
16. T. Futamase, Ki. Maeda, Phys. Rev. D **39**, 399–404 (1989)

17. D.S. Salopek, J.R. Bond, J.M. Bardeen, *Phys. Rev. D* **40**, 1753 (1989)
18. R. Fakir, W.G. Unruh, *Phys. Rev. D* **41**, 1783–1791 (1990)
19. L. Amendola, M. Litterio, F. Occhionero, *Int. J. Mod. Phys. A* **5**, 3861–3886 (1990)
20. D.I. Kaiser, *Phys. Rev. D* **52**, 4295–4306 (1995)
21. J.L. Cervantes-Cota, H. Dehnen, *Nucl. Phys. B* **442**, 391–412 (1995)
22. E. Komatsu, T. Futamase, *Phys. Rev. D* **59**, 064029 (1999)
23. Y. Akrami et al. (Planck), *Astron. Astrophys.* **641**, A10 (2020)
24. C.P. Burgess, H.M. Lee, M. Trott, *JHEP* **09**, 103 (2009)
25. J.L.F. Barbon, J.R. Espinosa, *Phys. Rev. D* **79**, 081302 (2009)
26. C.P. Burgess, H.M. Lee, M. Trott, *JHEP* **07**, 007 (2010)
27. M.P. Hertzberg, *JHEP* **11**, 023 (2010)
28. M.P. DeCross, D.I. Kaiser, A. Prabhu, C. Prescod-Weinstein, E.I. Sfakianakis, *Phys. Rev. D* **97**, 023526 (2018)
29. Y. Ema, R. Jinno, K. Mukaida, K. Nakayama, *JCAP* **02**, 045 (2017)
30. E.I. Sfakianakis, J. van de Vis, *Phys. Rev. D* **99**, 083519 (2019)
31. G.F. Giudice, H.M. Lee, *Phys. Lett. B* **694**, 294–300 (2011)
32. O. Lebedev, H.M. Lee, *Eur. Phys. J. C* **71**, 1821 (2011)
33. Y. Ema, *Phys. Lett. B* **770**, 403–411 (2017)
34. A. Salvio, A. Mazumdar, *Phys. Lett. B* **750**, 194–200 (2015)
35. S. Pi, Yl. Zhang, Q.-G. Huang, M. Sasaki, *JCAP* **05**, 042 (2018)
36. D. Gorbunov, A. Tokareva, *Phys. Lett. B* **788**, 37–41 (2019)
37. A. Gundhi, C.F. Steinwachs, *Nucl. Phys. B* **954**, 114989 (2020)
38. M. He, R. Jinno, K. Kamada, S.C. Park, A.A. Starobinsky, J. Yokoyama, *Phys. Lett. B* **791**, 36–42 (2019)
39. D.Y. Cheong, S.M. Lee, S.C. Park, *JCAP* **01**, 032 (2021)
40. F. Bezrukov, D. Gorbunov, C. Shepherd, A. Tokareva, *Phys. Lett. B* **795**, 657–665 (2019)
41. M. He, R. Jinno, K. Kamada, A.A. Starobinsky, J. Yokoyama, *JCAP* **01**, 066 (2021)
42. F. Bezrukov, C. Shepherd, *JCAP* **12**, 028 (2020)
43. M. He, *JCAP* **05**, 021 (2021)
44. G. Aad et al. (ATLAS), *Phys. Lett. B* **716**, 1–29 (2012)
45. S. Chatrchyan et al. (CMS), *Phys. Lett. B* **716**, 30–61 (2012)
46. G. Degrassi, S. Di Vita, J. Elias-Miro, J.R. Espinosa, G.F. Giudice, G. Isidori, A. Strumia, *JHEP* **08**, 098 (2012)
47. Y. Hamada, H. Kawai, Ky. Oda, S.C. Park, *Phys. Rev. D* **91**, 053008 (2015)
48. P. Zyla et al. (Particle Data Group), *PTEP* **2020**, 08301 (2020)
49. M. He, A.A. Starobinsky, J. Yokoyama, *JCAP* **05**, 064 (2018)
50. T. Modak, Ky. Oda, *Eur. Phys. J. C* **80**, 863 (2020)
51. J.-O. Gong, H.M. Lee, S.K. Kang, *JHEP* **04**, 128 (2012)
52. M.N. Dubinin, E.Y. Petrova, E.O. Pozdeeva, M.V. Sumin, S.Y. Vernov, *JHEP* **12**, 036 (2017)
53. S. Choubey, A. Kumar, *JHEP* **11**, 080 (2017)
54. L. Wang, [arXiv:2105.02143](https://arxiv.org/abs/2105.02143) [hep-ph]
55. A.A. Starobinsky, *JETP Lett.* **30**, 682–685 (1979)
56. A. Djouadi, *Phys. Rep.* **459**, 1–241 (2008)
57. G.C. Branco, P.M. Ferreira, L. Lavoura, M.N. Rebelo, M. Sher, J.P. Silva, *Phys. Rep.* **516**, 1–102 (2012)
58. S. Davidson, H.E. Haber, *Phys. Rev. D* **72**, 035004 (2005)
59. W.-S. Hou, M. Kikuchi, *EPL* **123**, 11001 (2018)
60. M. Sasaki, E.D. Stewart, *Prog. Theor. Phys.* **95**, 71–78 (1996)
61. D.I. Kaiser, A.T. Todhunter, *Phys. Rev. D* **81**, 124037 (2010)
62. J.O. Gong, T. Tanaka, *JCAP* **03**, 015 (2011)
63. C.M. Peterson, M. Tegmark, *Phys. Rev. D* **87**, 103507 (2013)
64. J. White, M. Minamitsuji, M. Sasaki, *JCAP* **07**, 039 (2012)
65. R.N. Greenwood, D.I. Kaiser, E.I. Sfakianakis, *Phys. Rev. D* **87**, 064021 (2013)
66. D.I. Kaiser, E.I. Sfakianakis, *Phys. Rev. Lett.* **112**, 011302 (2014)
67. S. Karamitsos, A. Pilaftsis, *Nucl. Phys. B* **927**, 219–254 (2018)
68. D.I. Kaiser, E.A. Mazenc, E.I. Sfakianakis, *Phys. Rev. D* **87**, 064004 (2013)
69. H. Kodama, M. Sasaki, *Prog. Theor. Phys. Suppl.* **78**, 1–166 (1984)
70. V.F. Mukhanov, H.A. Feldman, R.H. Brandenberger, *Phys. Rep.* **215**, 203–333 (1992)
71. K.A. Malik, D. Wands, *Phys. Rep.* **475**, 1–51 (2009)
72. M. Sasaki, *Prog. Theor. Phys.* **76**, 1036 (1986)
73. V.F. Mukhanov, *Sov. Phys. JETP* **67**, 1297–1302 (1988)
74. J. Elliston, D. Seery, R. Tavakol, *JCAP* **11**, 060 (2012)
75. R. Easther, J.T. Giblin, *Phys. Rev. D* **72**, 103505 (2005)
76. D. Langlois, S. Renaux-Petel, *JCAP* **04**, 017 (2008)
77. C.M. Peterson, M. Tegmark, *Phys. Rev. D* **83**, 023522 (2011)
78. C.M. Peterson, M. Tegmark, *Phys. Rev. D* **84**, 023520 (2011)
79. D. Wands, K.A. Malik, D.H. Lyth, A.R. Liddle, *Phys. Rev. D* **62**, 043527 (2000)
80. L. Amendola, C. Gordon, D. Wands, M. Sasaki, *Phys. Rev. Lett.* **88**, 211302 (2002)
81. D. Wands, N. Bartolo, S. Matarrese, A. Riotto, *Phys. Rev. D* **66**, 043520 (2002)
82. B.A. Bassett, S. Tsujikawa, D. Wands, *Rev. Mod. Phys.* **78**, 537–589 (2006)
83. S. Antusch, D. Nolde, S. Orani, *JCAP* **06**, 009 (2015)
84. B. Powell, W. Kinney, *JCAP* **08**, 006 (2007)
85. D. Eriksson, J. Rathman, O. Stal, *Comput. Phys. Commun.* **181**, 189–205 (2010)
86. W.-S. Hou, M. Kohda, T. Modak, *Phys. Rev. D* **99**, 055046 (2019)
87. T. Modak, *Phys. Rev. D* **100**, 035018 (2019)
88. W.-S. Hou, T. Modak, *Phys. Rev. D* **101**, 035007 (2020)
89. T. Modak, E. Senaha, *JHEP* **2011**, 025 (2020)
90. M.E. Peskin, T. Takeuchi, *Phys. Rev. D* **46**, 381–409 (1992)
91. M. Baak et al. (Gfitter Group), *Eur. Phys. J. C* **74**, 3046 (2014)
92. P. Ferreira, H.E. Haber, E. Santos, *Phys. Rev. D* **92**, 033003 (2015)
93. H.E. Haber, R. Hempfling, *Phys. Rev. D* **48**, 4280–4309 (1993)
94. B.A. Bassett, C. Gordon, R. Maartens, D.I. Kaiser, *Phys. Rev. D* **61**, 061302 (2000)
95. A.R. Liddle, D.H. Lyth, K.A. Malik, D. Wands, *Phys. Rev. D* **61**, 103509 (2000)
96. C. Gordon, D. Wands, B.A. Bassett, R. Maartens, *Phys. Rev. D* **63**, 023506 (2000)
97. P.A.R. Ade et al. (BICEP and Keck), *Phys. Rev. Lett.* **127**(15), 151301 (2021). <https://doi.org/10.1103/PhysRevLett.127.151301>. [arXiv:2110.00483](https://arxiv.org/abs/2110.00483) [astro-ph.CO]
98. T. Matsumura, Y. Akiba, J. Borrill, Y. Chinone, M. Dobbs, H. Fuke, A. Ghribi, M. Hasegawa, K. Hattori, M. Hattori et al., *J. Low Temp. Phys.* **176**, 733 (2014)
99. P. Ade et al. (Simons Observatory), *JCAP* **02**, 056 (2019)
100. W.-S. Hou, M. Kohda, T. Modak, *Phys. Rev. D* **98**, 075007 (2018)
101. The ATLAS collaboration, ATLAS-CONF-2020-027. <http://cds.cern.ch/record/2725733>
102. The CMS collaboration, CMS-PAS-HIG-19-005. <http://cds.cern.ch/record/2706103>
103. B. Altunkaynak, W.-S. Hou, C. Kao, M. Kohda, B. McCoy, *Phys. Lett. B* **751**, 135 (2015)
104.  $B_{d,s}$  measurements of UTfit collaboration. <http://www.utfit.org/UTfit/ResultsSummer2018NP>
105. R. Aaij et al. (LHCb), [arXiv:1808.08865](https://arxiv.org/abs/1808.08865) [hep-ex]
106. E. Kou et al. (Belle-II), *PTEP* **2019**, 123C01 (2019)
107. M. Aaboud et al. (ATLAS), *JHEP* **1905**, 123 (2019)
108. The CMS collaboration, CMS-PAS-TOP-20-007. <http://cds.cern.ch/record/2771683>
109. W.-S. Hou, T. Modak, T. Plehn, *SciPost Phys.* **10**, 150 (2021)
110. A. Crivellin, A. Kokulu, C. Greub, *Phys. Rev. D* **87**, 094031 (2013)
111. T. Modak, E. Senaha, *Phys. Rev. D* **99**, 115022 (2019)
112. W.-S. Hou, M. Kohda, T. Modak, G.-G. Wong, *Phys. Lett. B* **800**, 135105 (2020)
113. W.-S. Hou, T.-H. Hsu, T. Modak, *Phys. Rev. D* **102**, 055006 (2020)

114. The ATLAS collaboration, ATLAS-CONF-2020-039. <http://cds.cern.ch/record/2727860>
115. A.M. Sirunyan et al. (CMS), JHEP **2007**, 126 (2020)
116. M. Aaboud et al. (ATLAS), Phys. Rev. Lett. **119**, 191803 (2017)
117. A.M. Sirunyan et al. (CMS), JHEP **04**, 171 (2020)
118. D.K. Ghosh, W.-S. Hou, T. Modak, Phys. Rev. Lett. **125**, 221801 (2020)
119. A.M. Sirunyan et al. (CMS), Eur. Phys. J. C **80**, 75 (2020)
120. W.-S. Hou, M. Kohda, T. Modak, Phys. Lett. B **786**, 212 (2018)
121. W.-S. Hou, T. Modak, Mod. Phys. Lett. A **36**, 2130006 (2021)
122. M. Kohda, T. Modak, W.-S. Hou, Phys. Lett. B **776**, 379 (2018)
123. W.-S. Hou, M. Kohda, T. Modak, Phys. Lett. B **798**, 134953 (2019)
124. W.-S. Hou, T. Modak, Phys. Rev. D **103**, 075015 (2021)
125. J. Alwall et al., JHEP **1407**, 079 (2014)
126. R.D. Ball et al. (NNPDF Collaboration), Nucl. Phys. B **877**, 290 (2013)
127. T. Sjöstrand, S. Mrenna, P. Skands, JHEP **0605**, 026 (2006)
128. J. de Favereau et al. (DELPHES 3 Collaboration), JHEP **1402**, 057 (2014)
129. G. Cowan, K. Cranmer, E. Gross, O. Vitells, Eur. Phys. J. C **71**, 1554 (2011)
130. S.M. Lee, Ky. Oda, S.C. Park, JHEP **03**, 083 (2021)
131. V. Andreev et al. (ACME), Nature **562**(7727), 355–360 (2018)
132. S. Watanuki et al. (Belle), Phys. Rev. D **99**, 032012 (2019)
133. Y. Hamada, K. Kawana, A. Scherlis, JCAP **03**, 062 (2021)